

**IMPERIAL COLLEGE LONDON**

**Department of Earth Science and Engineering**

**Centre for Petroleum Studies**

**MODELLING MULTIPHASE FLOW  
USING A DYNAMIC PORE NETWORK MODEL FOR IMBIBITION**

**By**

**Sébastien Charonnat**

**A report submitted in partial fulfilment of the requirements  
for the MSc and/or the DIC.**

**September 2012**

September 2012

## DECLARATION OF OWN WORK

I declare that this thesis

**“Modelling Multiphase Flow using a Dynamic Pore Network Model for Imbibition”**

is entirely my own work and that where any material could be construed as the work of others, it is fully cited and referenced, and/or with appropriate acknowledgement given.

Signature: .....

Name of student: **Sébastien Charonnat**

Name of supervisor: **Prof. Martin J. Blunt**

Company supervisor: **Dr.Evren Unsal**

---

**Abstract**

This article presents a dynamic pore network model (PNM) for imbibition which is able to predict the displacement of oil by the injection of water in a porous medium. Developing such a model is done to, at term, be able to predict residual oil saturations and relative permeability without going through the time and money consuming core experiments. The model presented is an improvement of an existing code which originally only uses circular cross-sections, with no wetting film layers and constant contact angles.

The first part presents what makes this model and shows the formulae that allow the model to take into account capillary and viscous effects while calculating the pressure in both water and oil phases in each network element. The model has been implemented to allow its users to select the type of shape (circle, square or equilateral triangle) for the pores and throats' cross-sections, the type of contact angle distribution (constant, random, normal or log-normal) and all the parameters that quantify the fluids and their flow (oil and water viscosities, injection rate and interfacial tension).

In the second part, the simulator is validated using various 2-D network models. A qualitative validation of this pore network model is done by verifying the consistency of the type of displacement compared to flow patterns (viscous fingering, capillary fingering and piston-like displacement) observed in laboratory experiments and other PNM models. Variations of the capillary number, which is the ratio of viscous effects to capillary effects, and/or of the viscosity ratio, are done to find the different displacements types. The residual phase saturations at different capillary numbers have been compared. Some 3-D results are also shown.

**Acknowledgements**

I would like to thank all those who have made the completion of this project possible:

Firstly I wish to thank Dr.Evren Unsal, Prof. Olivier Gosselin, Dr.Dick Kachuma and Pierre Bergey of Total E&P UK who gave me the opportunity and helped me work on such an interesting project.

I was honoured to have Prof. Martin Blunt as academic supervisor.

I would also like to thank the French crew who made this year a pleasant one and our SPE committee for the trip to Brazil with all the unforgettable memories that came with it.

I am also very grateful to my parents and brothers for their overall support.

Last but not least a special thanks to Marine for being who you are.

---

**Table of Contents**

DECLARATION OF OWN WORK .....	2
Abstract .....	3
Acknowledgements .....	4
Table of Figures & Tables.....	6
Table of Figures & Tables - Appendices .....	6
<b>Modelling Multiphase Flow using a Dynamic Pore Network Model for Imbibition .....</b>	<b>7</b>
Abstract .....	7
Introduction.....	7
Description of the model.....	8
Calculation formulae used in model.....	9
Results achieved.....	10
Initial conditions and flow conditions .....	10
Geometry of (Lenormand et al. 1988)'s network .....	11
100*100 network.....	11
25*25 network.....	17
Geometry of (Unsal et al. 2011)'s network .....	17
Results with a 3D network .....	19
Discussion & Conclusion.....	20
Nomenclature .....	20
Subscripts .....	21
Reference .....	21
Appendix A – Literature review and bibliography .....	22
MILESTONES IN MULTIPHASE FLOW PORE SCALE NETWORK MODELLING .....	22
Appendix B – User Interface.....	56
Appendix C – 100*100 network simulation .....	58
Appendix D – 25*25 network simulation .....	60
Appendix E – 3D Simulations.....	64

## Table of Figures & Tables

Figure 1: Different types (circle, square and equilateral triangle cross-sections) of pores and throats .....	8
Figure 2: Appearance of wetting fluid films in pores with angular cross-sections. ....	8
Figure 3: 100*100 network with pore and throats with square cross-sections: Air (white) displacing viscous oil at various $C$ at $\log M = -4.7$ : from viscous fingering to capillary fingering. The first and third columns represent the results achieved by current PNM simulator and the second and fourth are the laboratory experiments by (Lenormand et al. 1988). ....	11
Figure 4: 100*100 network with pore and throats with square cross-sections: Mercury (black) displacing air at $\log M = 1.9$ : from piston-like displacement to capillary-fingering. The first and third columns represent the results achieved by current PNM simulator and the second and fourth are the laboratory experiments by (Lenormand et al. 1988). ....	12
Figure 5: Location on the $\log M - \log Ca$ plane of the simulations. ....	12
Figure 6: 100*100 simulations while varying the capillary numbers: (a) $\log M = -4.7$ from viscous fingering to capillary fingering. The first and third columns represent the results achieved and the second and fourth are the simulations by (Lenormand et al. 1988). ....	13
Figure 7: 100*100 network: Comparison between square (left) and circular (right) cross-sections. ....	13
Figure 8: 100*100 simulations while varying the capillary numbers: (b) $\log M = 1.9$ from piston-like displacement to capillary fingering. The first and third columns represent the results achieved and the second and fourth are the simulations by (Lenormand et al. 1988). ....	14
Figure 9: 100*100 simulations while varying the viscosity ratio: (c) $\log Ca = 0$ . The first and third columns represent the results achieved and the second and fourth are the simulations by (Lenormand et al. 1988). ....	15
Figure 10: 100*100 simulations: plot of the injected fluid saturation when it has crossed the entire network; the points represent the results of the simulations and those by (Lenormand et al. 1988). ....	16
Figure 11: 25*25 simulations: plot of the injected fluid saturation when it has crossed the entire network. ....	17
Figure 12: 120*80 simulations while varying the capillary number for $M > 1$ . The first row is the experiments and the second row results achieved. Orange represents the liquid injected. ....	18
Figure 13: 120*80 simulations while varying the capillary number for $M < 1$ . The first row is the experiments and the second row results achieved. Orange represents the liquid injected. ....	18
Figure 14: 3D network simulations: plot of the injected fluid saturation when it has crossed the entire network. In red are the cases where the pictures of the flow in the network are provided. ....	19
Figure 15: Viscous fingering in the carbonate C1 (provided by ICL) obtained at $\log Ca = -4$ and $\log M = -2$ . Blue corresponds to the water injected and green to the oil initially in place. ....	19
Figure 16: Piston-like displacement in the carbonate C1 (provided by ICL) obtained at $\log Ca = -1$ and $\log M = 2$ . Blue corresponds to the water injected and green to the oil initially in place. ....	20
Figure 17: Water relative permeability curves obtained for the viscous fingering (on the left) and the piston like-displacement (on the right) in the carbonate C1 (provided by ICL). ....	20
Table 1: Parameters from the Hagen-Poiseuille formula, which depend on the type of cross-section. ....	10
Table 2: Summary of the model improvements. ....	10
Table 3: Parameters used for the 120*80 simulations at a constant $M = 0.25$ . ....	17
Table 4: Parameters used for the 120*80 simulations at a constant $M = 15$ . ....	17

## Table of Figures & Tables - Appendices

Figure B- 1: Window in which you enter the imbibition parameters you wish to run your simulation for. ....	56
Figure B- 2: Help window explaining what all the imbibition parameters correspond to. ....	57
Figure C- 1: 100*100 simulations while varying the capillary numbers: (a) $\log M = -4.7$ . Small $Ca$ are simulated in order to reach the capillary fingering plateau. ....	58
Figure C- 2: 100*100 simulation while varying the viscosity ratios: (c) $\log Ca = 0$ . A big viscosity ratio is simulated in order to reach the piston-like displacement plateau. ....	59
Figure D- 1: 25*25 simulations while varying the capillary numbers: (a) $\log M = -4.7$ . Small $Ca$ are simulated in order to reach the capillary fingering plateau. ....	60
Figure D- 2: 25*25 simulations while varying the capillary numbers: (a) $\log M = 1.9$ . Small $Ca$ are simulated in order to reach the capillary fingering plateau. ....	61
Figure D- 3: 25*25 simulation while varying the viscosity ratios: (c) $\log Ca = 0$ . A big viscosity ratio is simulated in order to reach the piston-like displacement plateau. ....	62
Figure D- 4: 25*25 simulation while varying the viscosity ratios: (c) $\log Ca = -6.5$ . A small viscosity ratio is simulated in order to reach the viscous fingering plateau. ....	63
Table C- 1: Parameters used for the 100*100 simulations at a constant $\log M = -4.7$ . ....	58
Table C- 2: Parameters used for the 100*100 simulations at a constant $\log Ca = 0$ . ....	58
Table D- 1: Parameters used for the 25*25 simulations at a constant $\log M = -4.7$ . ....	60
Table D- 2: Parameters used for the 25*25 simulations at a constant $\log M = 1.9$ . ....	61
Table D- 3: Parameters used for the 25*25 simulations at a constant $\log Ca = 0$ . ....	62
Table D- 4: Parameters used for the 25*25 simulations at a constant $\log Ca = -6.5$ . ....	63
Table E- 1: Parameters used for the 3D simulations at a constant $\log M = -2$ . ....	64
Table E- 2: Parameters used for the 3D simulations at a constant $\log M = 2$ . ....	64

# Modelling Multiphase Flow using a Dynamic Pore Network Model for Imbibition

Sébastien Charonnat

Imperial College supervisor: **Professor Martin Blunt**

Company supervisor: **Dr. Evren Unsal**

---

## Abstract

This article presents a dynamic pore network model (PNM) for imbibition which is able to predict the displacement of oil by the injection of water in a porous medium. Developing such a model is done to, at term, be able to predict residual oil saturations and relative permeability without going through the time and money consuming core experiments. The model presented is an improvement of an existing code which originally only uses circular cross-sections, with no wetting film layers and constant contact angles.

The first part presents what makes this model and shows the formulae that allow the model to take into account capillary and viscous effects while calculating the pressure in both water and oil phases in each network element. The model has been implemented to allow its users to select the type of shape (circle, square or equilateral triangle) for the pores and throats' cross-sections, the type of contact angle distribution (constant, random, normal or log-normal) and all the parameters that quantify the fluids and their flow (oil and water viscosities, injection rate and interfacial tension).

In the second part, the simulator is validated using various 2-D network models. A qualitative validation of this pore network model is done by verifying the consistency of the type of displacement compared to flow patterns (viscous fingering, capillary fingering and piston-like displacement) observed in laboratory experiments and other PNM models. Variations of the capillary number, which is the ratio of viscous effects to capillary effects, and/or of the viscosity ratio, are done to find the different displacements types. The residual phase saturations at different capillary numbers have been compared. Some 3-D results are also shown.

## Introduction

The first time a network of pores was used to represent multiphase flow in porous media was in the 1950s (Fatt 1956). Several types of pore network models have been developed since then. There are the quasi-static models (Øren et al. 1998; Patzek 2001; Blunt et al. 2002; Valvatne and Blunt 2004) which are based on the assumption that the capillary pressure is the only force controlling the pore-scale configurations of fluid and the displacement sequence. These models become limited for flows where viscous effects become important, i.e. high viscosity ratio, high injection rates. Dynamic models take into account such effects but computational costs become more expensive. Some of them track the positions at each time step of all menisci and their synchronous small displacement steps (Koplik and Lasseeter 1985) while others move one meniscus at a time to fill entire sections of the void space (Lenormand et al. 1988; Hammond and Unsal 2012). The latter is more approximate, but less time consuming.

In multiphase flow through angular pores and throats, the non-wetting phase is present in the centre of them, while the wetting phase stays in the angles and crevices of roughness in the pore space (Lenormand and Zarcone 1984). Flow through these wetting layers happens, which can result in a modification of the displacement type. For the particular case of imbibition, the displacement type is driven by the competition between the piston-like advance of the wetting fluid that fills entirely all pores and throats and snap-off where thinner regions of the pore network get swept before the connected front through flow in wetting layers (Lenormand et al. 1988).

This article presents a model that permits the prediction of how the oil will be displaced in a pore network model which will be injected with water. The model is a dynamic pore network simulator of the displacement of oil by water moving one meniscus at a time while capturing both the effects of capillary and viscous effects. Developing such a model is done to, at term, be able to predict residual oil saturations and relative permeability without going through the time and money consuming lab experiments.

The simulations run on a simplified model of how the pore space actually is and the calculation steps of the water progression are done on an individual filling events basis. The phase saturations and relative permeability functions are calculated from the size and the distribution of the pores and throats and through the resulting pressures, water concentrations and flows. The cross checking of the validity of the model is based on (Lenormand et al. 1988) and (Unsal et al. 2011)'s work by verifying if the flow pattern gotten (viscous fingering, capillary fingering or piston-like displacement) is consistent with what they had and by comparing the injected fluid saturation profile versus either  $\log Ca$  (capillary number) or  $\log M$  (viscosity ratio).

### Description of the model

The model developed during this project is an improvement of an existing code which originally only uses circular cross-sections (Purcell 1949). In the previous model each pore or throat could only contain one phase at a time. After the new implementation, it can now work with square and equilateral triangle cross sections (Pickell 1966; Singhal and Somerton 1970; Kwon and Pickett 1975) (Figure 1) that allow two fluids to be simultaneously present in one pore or throat: non-wetting phase in the centre and wetting films (Tuller et al. 1999) in the angular corners (Figure 2). Even if those geometrical shapes do not accurately represent the real pore networks, the introduction of wetting layers is important in the process of representing what really happens in a pore network regarding the modelling of the snap-off phenomenon or, more simply, the flow in those wetting layers. To surmount numerical difficulties associated with a dynamic model, it was assumed that the wetting films did not swell.

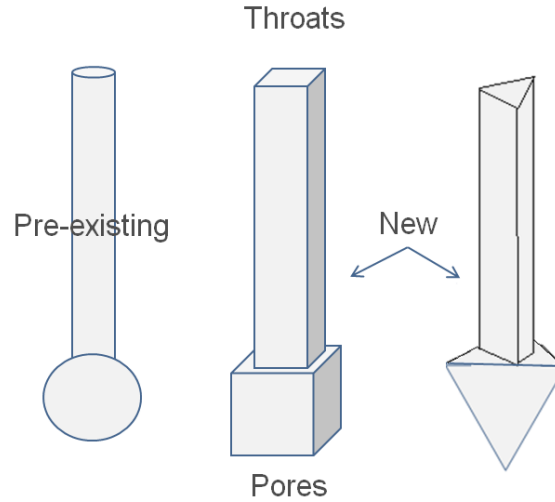


Figure 1: Different types (circle, square and equilateral triangle cross-sections) of pores and throats

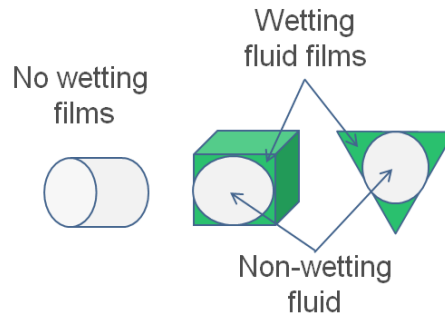


Figure 2: Appearance of wetting fluid films in pores with angular cross-sections.

In the pores and throats of the network, the displacement of one fluid by another is not only controlled by the pore' and throat's geometrical properties. It is also controlled by the pressures inside the two fluids (viscous effects), the interfacial tension between them and the contact angle with the surface of the elements (static effects). The flow controlling properties such as the threshold oil–water pressure difference and the hydraulic conductance are determined with the elements fixed geometrical properties. In this work, it is assumed that the interface between oil and aqueous phases is well-defined and sharp. Meanwhile, the effect of the interfacial area at the oil/water interphase (Joekar-Niasar et al. 2010) is not included. Also, one of the particularities of this model is that the oil and water pressures are calculated separately in each network elements.

This model is dynamic and the effects of viscous effects in both phases are considered in each element. The presence of viscous effects is especially important when a low viscosity fluid is injected into a high viscosity one, like in heavy oil. The Nguyen et al. (2004; 2005) technique of taking the pressures within the oil filled pores as spatially uniform and only computing the pressure gradients within the water films is not accurate enough since the effect of viscosity ratio is not noticeable except if the pressure gradients are computed within the two phases. In immiscible flow, the displacement pattern is highly influenced by the viscosity ratio between the displaced and displacing liquids. Simulations are therefore strongly sensitive to the viscosity (mobility) ratio,

$$M = \mu_w/\mu_o \quad (1)$$

Pores and throats can be filled by both fluid residing in the centres of pores and throats next to it or by swelling and snapping-off of wetting films. The first type of displacements is piston-like displacements and the other is snap-off. When



capillary effects decrease as the displacement progresses, the wetting films in the corners of elements swells. At some point, if the film swells and is no longer in contact with the contact surface, the non-wetting fluid becomes unstable and snaps-off. Snap-off does not occur at all for contact angles  $\theta$  greater than  $45^\circ$ . It only occurs in parts of the pore network where the piston-like displacement cannot take place because the capillary pressure for snap-off is lower than the capillary pressure for piston-like displacement.

In order to minimize the calculation time, the movements of the menisci are updated every time a pore or throat is completely filled by the invading fluid rather than simulating the instant motion of all the menisci simultaneously within the network elements. It means that the elements are either initially filled by oil and a thin water film or fully occupied by water: no intermediate states are actually represented. The simulator does not account for ganglion dynamics (Constantinides and Payatakes 1991). The sequential approach used in this case is valid mainly in network modelling of capillary-dominated processes.

What makes the displacement events happen relies on the relationship between the (Hughes and Blunt 2000)'s threshold for capillary pressure and the difference between the local values of the oil and water pressures. The capillary pressure threshold used depends on the local oil–water interfacial tension  $\sigma$ , the local geometry of the element, and the local oil–water wettability contact angle,  $\theta$ . That criterion for displacement is used in order to know when an injected water meniscus displaces and enters the previously oil filled element. Wherever an oil displacement is feasible, the local difference in pressure between the oil and water phases is compared to the local geometrically determined threshold pressure for displacement. The element selected for displacement is the one in which the local difference in pressure exceeds the most the threshold (Idowu and Blunt 2010). The displacement selection criterion chosen is said to be exact, as the pressures for each feasible displacement are all evaluated and compared. The equation that applies for the displacement is:

$$\Delta P = P_c - (P_{non-wetting} - P_{wetting}) \quad (2)$$

To determine the relative importance of viscous to static effects, the capillary number is used and defined as:

$$Ca = \mu_w \cdot q_{inw} / (\Sigma \cdot \sigma_{ow} \cdot \cos(\theta)) \quad (3)$$

where  $\mu_w$  is the viscosity of the injected aqueous phase ( $\mu_o$  is the oil viscosity),  $\sigma_{o-w}$  is the oil–water interfacial tension,  $\Sigma$  is the cross-sectional area of the sample and  $q_{inw}$  the rate at which the water is injected into the network.  $\Sigma$  is the product of the width of the network by the distance between two sites.

The fluid injection rate is the process controlling the simulation. It was assumed that the wetting films did not swell meaning that they did not increase over any time period. The centres of pores and throats are filled with oil with water in the corners. The pressure at the exit is set to zero. The oil is connected to the outlet and can leave the network, so can the water. The simulation stops when no more moves in the network are possible.

Since the cross-section area affects the capillary effects (Eq. 3), if the shapes of the cross-sections were modified, it implied changes in the formulas that allow the calculation of the conductances and the capillary pressures in the network. In the next section, the formulas of such effects will be shown.

### Calculation formulae used in model

From Eqs (2) and (3) it can be seen that the injection rate and the fluid viscosities affect the viscous effects, and consequently the displacement patterns. The interfacial tension and the contact angle on the other hand, affect the capillary effects. The pressure in the wetting films are affected the same way: the pressure in them is calculated at every time step, but their capillary pressure calculation is different:

To calculate the capillary pressure for snap-off for regular polygons (Hughes and Blunt 2000)'s threshold was used:

$$P_{c,s} = \frac{\sigma}{r_{t/p}} (\cos \theta - \sin \theta \tan \alpha) \quad (4)$$

where  $r_{t/p}$  is the throat or pore radius,  $\alpha$  is the half-angle of the corners and  $\theta$  is the wettability contact angle.

In the case of contact angles superior to  $45^\circ$ , meaning that snap-off will not occur, the threshold used for frontal filling of pores and throats was:

$$P_c = 2 * \frac{\sigma}{r_{t/p}} * \cos \theta \quad (5)$$

The conductance  $h_c$  was calculated using the Hagen-Poiseuille formula:

$$h_c = k \frac{A^2 G}{\mu_{t/p}} \quad (6)$$

The  $k$  is a constant depending on the shape of the cross-section,  $A$  corresponds to the cross-sectional area and  $G = A/P^2$  is the shape factor (Mason and Morrow, 1991) with  $P$  representing the perimeter length of the shape. All the values of those constants are defined in Table 1.

**Table 1: Parameters from the Hagen-Poiseuille formula, which depend on the type of cross-section.**

Cross-section shape	Circle	Equilateral Triangle	Square
$\alpha$	-	30°	45°
$k$	0.5	3/5	0.5623
$G$	$\frac{1}{4\pi}$	$\frac{\sqrt{3}}{36}$	$\frac{1}{16}$
$A$	$\pi * r_t^2$	$3^{1.5} * r_t^2$	$4 * r_t^2$

The cross-sectional area occupied by wetting fluid in a pore or throat is given by (Oren et al. 1998)'s formula:

$$A_w = r_{t/p}^2 \left( \frac{\cos \theta \cos(\theta + \alpha)}{\sin \alpha} + \alpha + \theta - \frac{\pi}{2} \right) \quad (7)$$

With  $r_{t/p}$  taken has the throat or pore radius.

The conductance for the wetting layers was given by:

$$h_{cw} = \frac{A_{w-t/p}}{A} h_c \quad (8)$$

The code has also been implemented to allow the wettability contact angles in each pore or throat to be either fixed to a constant value, to vary randomly, to follow a normal distribution or a lognormal distribution.

This feature and all of the ones presented previously are summarized and compared with (Lenormand et al. 1988) and (Idowu and Blunt 2010)'s models in Table 2 and can all be easily chosen through a user interface.

**Table 2: Summary of the model improvements**

Lenormand et al. 1988's model	TOTAL's Original Model	TOTAL's Improved Model	Idowu and Blunt 2010's model
Dynamic	Dynamic		Dynamic
Circular Cross-Sections	Circular Cross-Sections	→ Angular Cross-Sections	Angular Cross-Sections
No Films	No Films	→ Wetting-Phase Films	Wetting-Phase Films
Fixed Contact Angles	Fixed Contact Angles	→ Contact Angle Distribution	Contact Angle Distribution

## Results achieved

To validate the implementation of the pore network multiphase flow model, (Lenormand et al. 1988) and (Unsal et al. 2011) experiments were used as references. A comparison with (Lenormand et al. 1988)'s simulations is also done. Following the validation, a presentation of results achieved on a 3D network is provided.

## Initial conditions and flow conditions

For all of the porous mediums used, it was assumed that they were all initially saturated with the wetting phase. They were then invaded with the non-wetting phase and drained completely. Only the wetting films in the corners stayed and the wetting layer is therefore always connected. The networks are close to be initially 100% oil saturated and the wetting fluid is injected from the left hand side. The network is horizontal. The outlet is on the right hand side. Side surfaces are no-flow boundaries. Gravity effects are neglected. The fluids are assumed to be incompressible and the viscosities are assumed to be constant.

With the dimensionless numbers that are the capillary number and the viscosity ratio, ratios defined in the Description of the model section, which are the ratios of two different effects, a simulation is characterized. Therefore, each simulated displacement can be represented as a point on a plane that has for axes the logarithm of the viscosity ratio and the logarithm of the capillary number.

The flow patterns that are going to be encountered are the following:

- **Viscous fingering** which is the formation of patterns in a morphologically unstable interface between two fluids in a porous medium. The principal effect is due to when a less viscous fluid is injected displacing a more viscous one. The fingers don't make much deviation in their way towards the exit.
- **Capillary fingering** that has for principal effect acting capillarity. The fingers also spread towards the exit but while they do so, they expand laterally and therefore trap the displaced oil. The final saturation of the liquid injected is higher than in the previous case.
- **Piston-like displacement** which presents a pattern of a flat front with very little liquid in place trapped. The principal force is due to when a more viscous fluid is injected displacing a less viscous one.

### Geometry of (Lenormand et al. 1988)'s network

The porous medium is represented by a square two-dimensional lattice with pores linked with neighbour pores by throats. The pores can be spherical, triangular or cubes but in this paper, only the results achieved with the cubical pores are presented. As for the throats, their cross-sections can be a circle, an equilateral triangle or a square but only the square case is shown. Every element is defined by its radius that is assigned to each one of them by following a normal distribution centred on the average radius  $r_0$ . To characterize a network, the mean radius and the standard deviation for the distribution for the pores and throats plus the distance between two pores are the parameters necessary.

To be consistent with (Lenormand et al. 1988)'s work, a network of (100\*100) and one of (25\*25) are used. The larger one is computer-time consuming but its size is close to the one used in experimental micromodels and the small one allows more simulations to be ran and therefore the M-Ca plane can be further explored.

#### 100\*100 network

Their grids representing the pore-networks were statistically reproduced. The mean radius of the pores is equal to the mean radius of the throats  $r_0 = 0.23$  mm with a standard deviation of 0.5 for the throats and 0.2 for the pores. The same grid is used for all simulations.

#### a. Comparison with the laboratory experiments (100\*100 network)

The first series of simulation that is compared with experiments is done at a constant  $\log M = -4.7$  while varying Ca (Figure 3). This experiment corresponds to the injection of air into a viscous oil filled network.

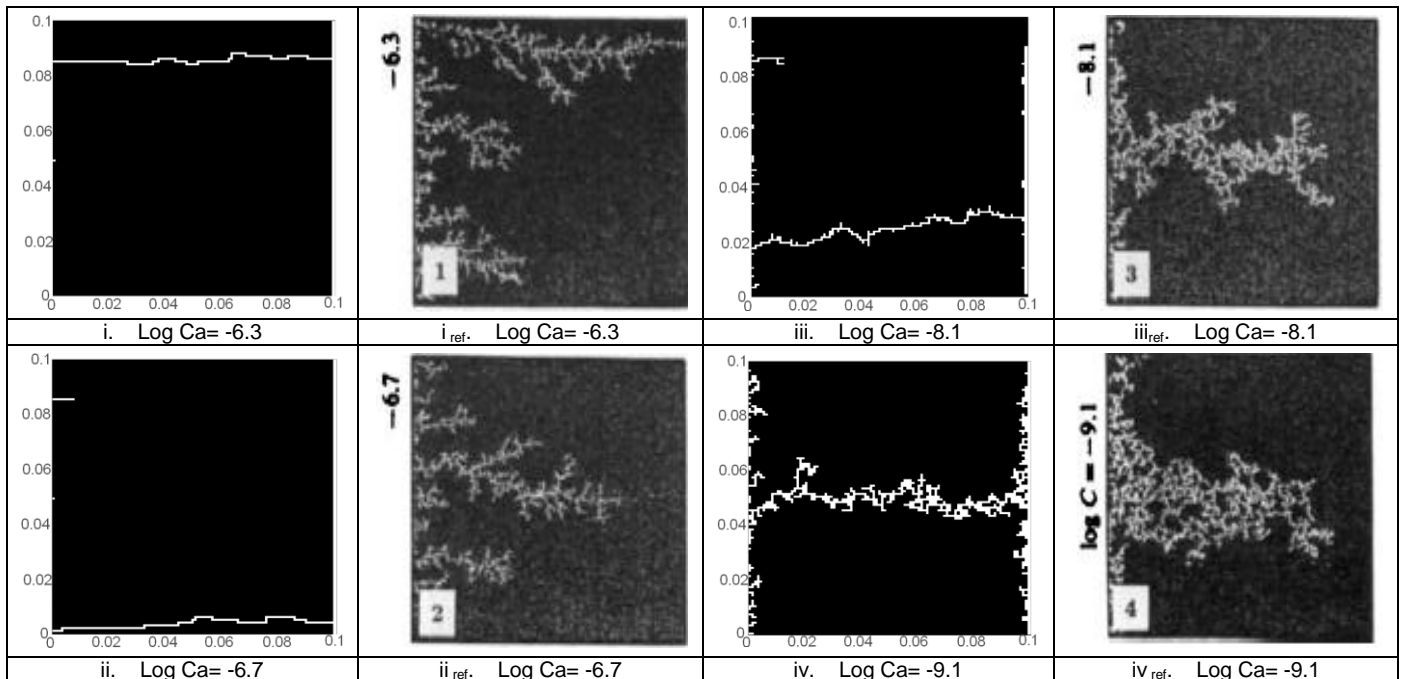


Figure 3: 100\*100 network with pore and throats with square cross-sections: Air (white) displacing viscous oil at various C at  $\log M = -4.7$ : from viscous fingering to capillary fingering.

The first and third columns represent the results achieved by current PNM simulator and the second and fourth are the laboratory experiments by (Lenormand et al. 1988).

The results with the current PNM and the corresponding experiment are plotted left and right respectively. The transition from viscous fingering (cases i. and ii.) to capillary fingering (cases iii. and iv.) is visible. This transition happens for nearly the same capillary numbers as for the experiments. Meanwhile, it can be noted that the fingers do not expand as much in the simulations than in the experiments. Apart from that last aspect, the behaviour of the simulations at a constant  $\log M = -4.7$  is consistent with the lab results.

The second series of simulation that is compared with experiments is done at a negative mobility number  $\log M = -1.9$  while varying  $Ca$  (Figure 4). This experiment corresponds to the injection of mercury into an air filled network.

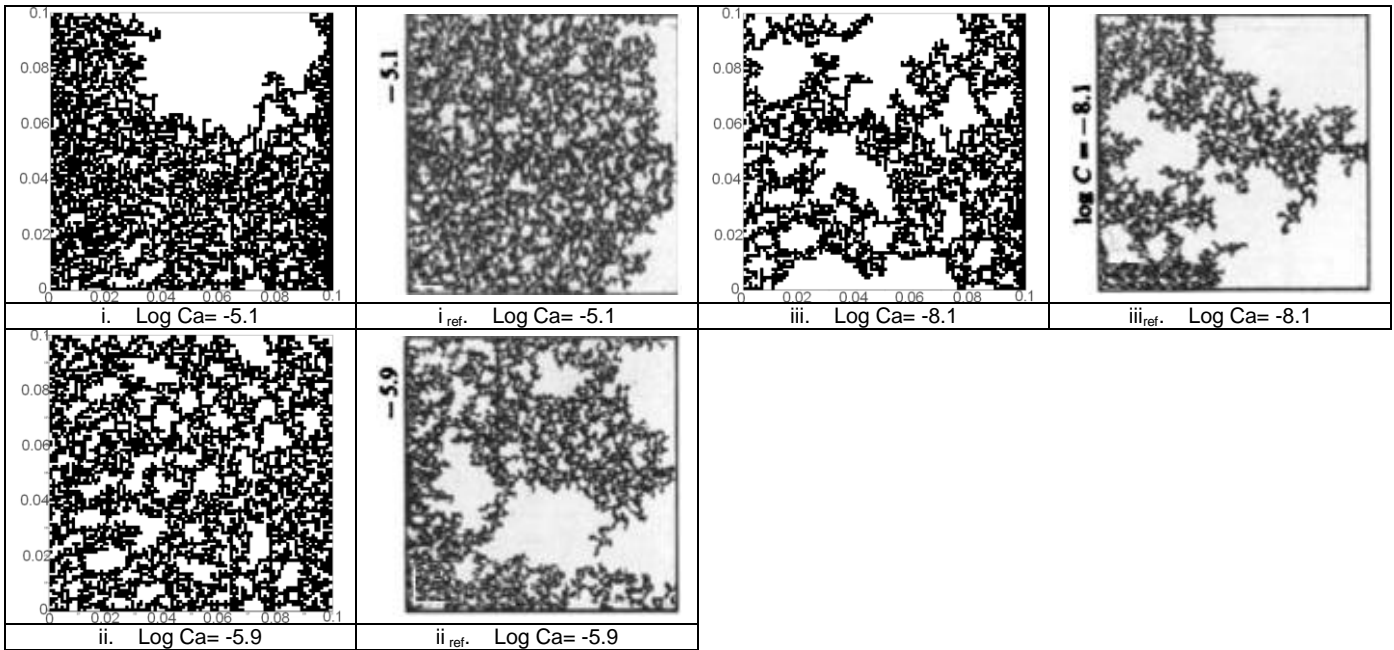


Figure 4: 100\*100 network with pore and throats with square cross-sections: Mercury (black) displacing air at  $\log M = 1.9$ : from piston-like displacement to capillary-fingering.

The first and third columns represent the results achieved by current PNM simulator and the second and fourth are the laboratory experiments by (Lenormand et al. 1988).

The first case is with the highest injection rate and, as opposed to Figure 3, no fingering can be seen. Instead, a lot of small oil clusters trapped in water can be observed. As the injection decreases, the trapped oil clusters get larger and fewer in quantities. The simulation results are consistent the experiments.

*b. Comparison with the simulation results (100\*100 network)*

The simulations are run as two series at different  $Ca$  and constant  $M$  and a series at constant  $Ca$  and varying  $M$ . The summary of all simulations with their  $Ca$  and  $M$  numbers associated are shown Figure 5. In total there are 20 cases that have been tested and are presented.

While comparing with (Lenormand et al. 1988)'s simulation, it was taken into consideration that some of the results they had would be different since they assume that and that their pores and throats have circular cross-sections (so no corners and no wetting fluid layer flow), in contrast to this work.

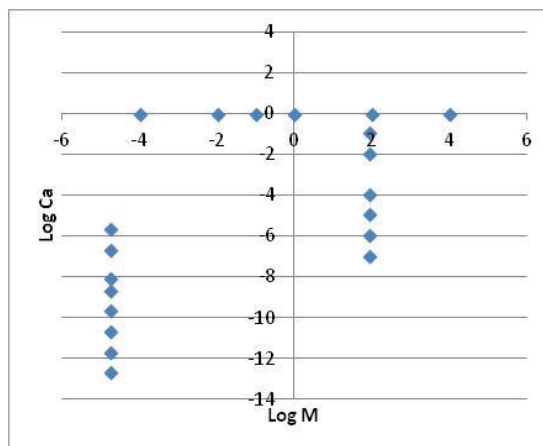
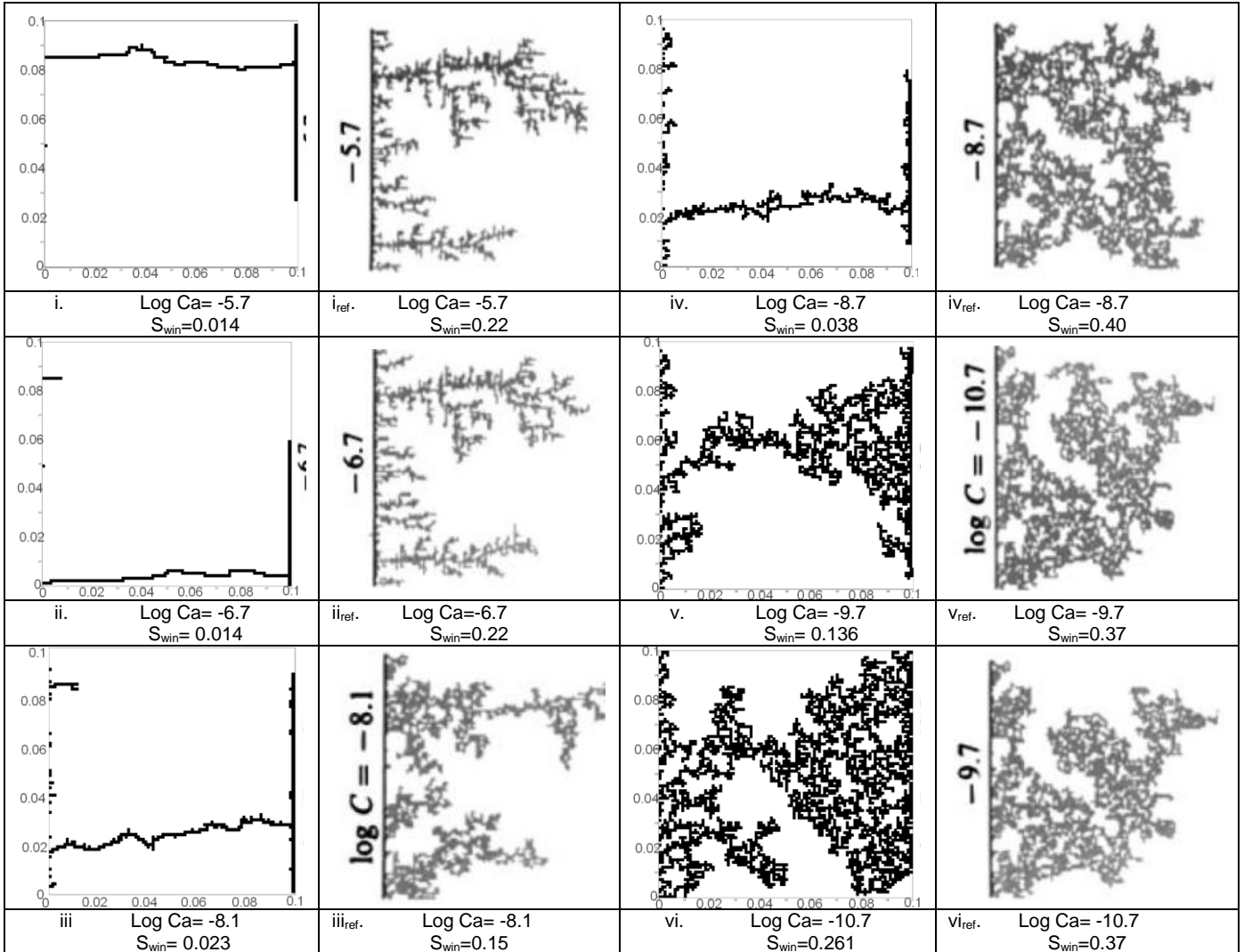


Figure 5: Location on the  $\log M - \log Ca$  plane of the simulations.

In Figure 6, Figure 7, Figure 8 and Figure 9 the black corresponds to the pores and throats filled with injected fluid and the white to the ones filled with fluid in place.

The first series of simulations, a less-viscous fluid than the one in place is injected ( $\log M = -4.7$ ) and the injection flow rate is decreased.



**Figure 6:**  $100 \times 100$  simulations while varying the capillary numbers: (a)  $\log M = -4.7$  from viscous fingering to capillary fingering. The first and third columns represent the results achieved and the second and fourth are the simulations by (Lenormand et al. 1988).

At high flow rates the pattern seen corresponds to viscous fingering while at very low Ca, the pattern is capillary fingering. For the viscous fingering (Figure 6 i. and ii.) in the model, the flow takes a more direct route than for (Lenormand et al. 1988)'s one. As the injection rate decreases, the capillary effects take over and more branching of the water phase is observed (Figure 6 v. and vi.). The capillary fingering forms here at a lower Ca. It can be explained by the existence of flow in the connected wetting layer in this model. This affirmation can be justified by comparing in Figure 7 the flow pattern of capillary fingering that is far more developed in the absence of a wetting-layer (i.e. for circular cross-sections) than when it exists (i.e. for square cross-sections).

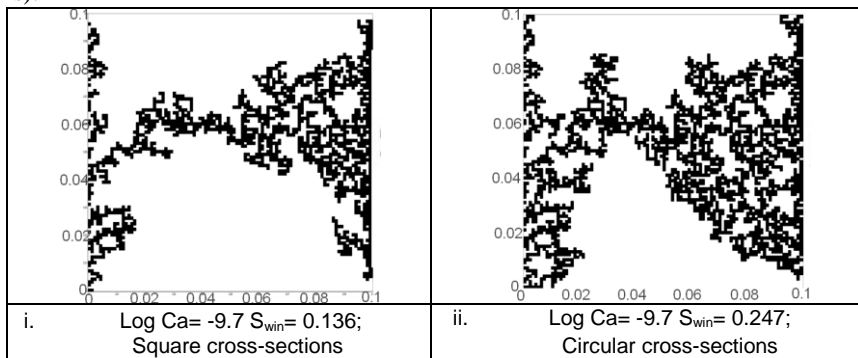


**Figure 7:**  $100 \times 100$  network: Comparison between square (left) and circular (right) cross-sections.



The second series of simulations are made using the same 100x100 network while injecting a more-viscous fluid than the one in place ( $\log M = 1.9$ ). The results are shown in order of decreasing Ca (Figure 8).

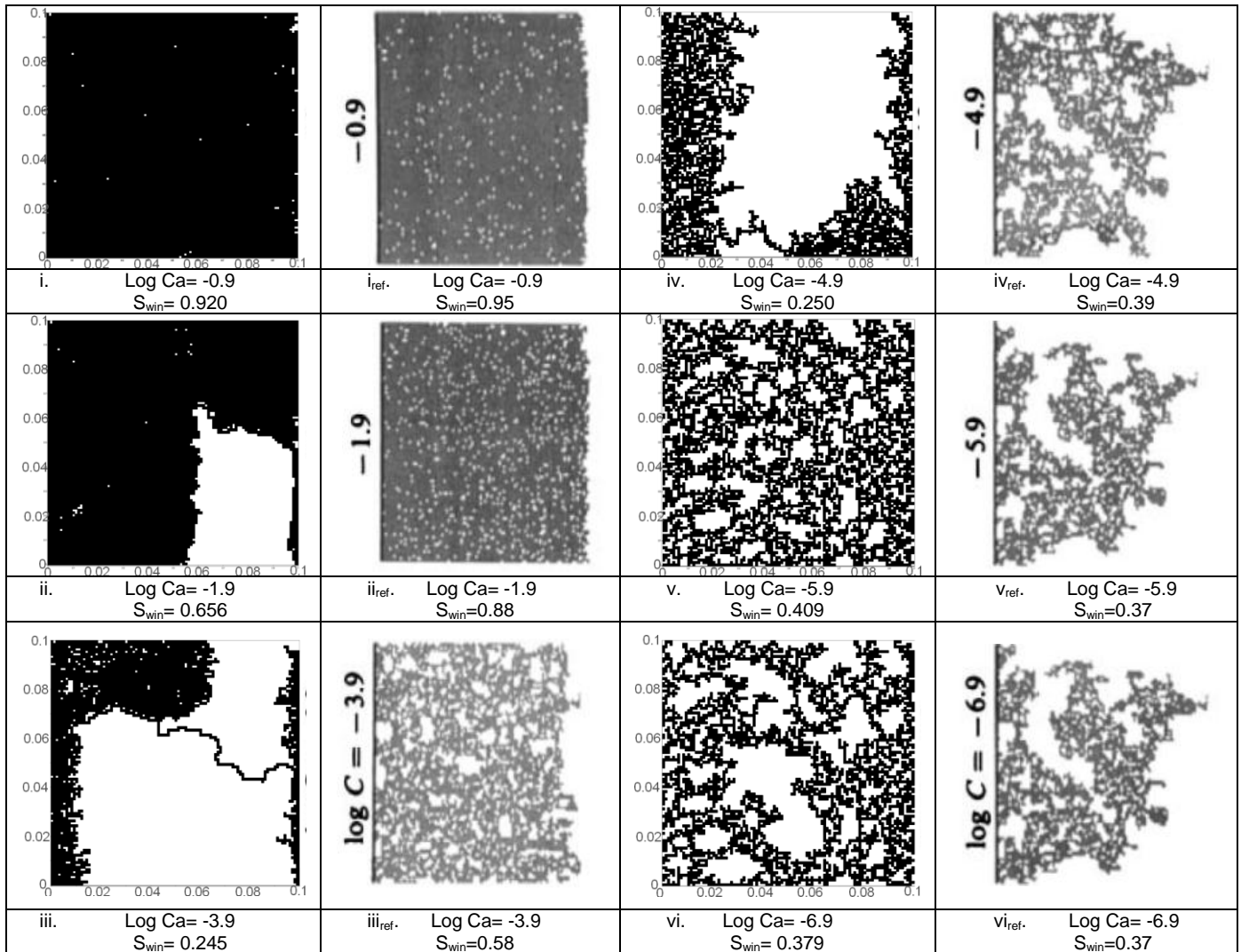


**Figure 8: 100\*100 simulations while varying the capillary numbers: (b)  $\log M = 1.9$  from piston-like displacement to capillary fingering. The first and third columns represent the results achieved and the second and fourth are the simulations by (Lenormand et al. 1988).**

At very low Ca, the capillary effects are dominant and piston-like displacement is the pattern that can be seen at higher flow rates. The piston-like displacement achieved in (Figure 8 i.) is exactly what was expected but the one in (Figure 8 ii.) shows in the bottom right part of the network a large oil blob was trapped. The same sort of bug appears in the (Figure 8 iii. and iv.) where the capillary fingering progresses too fast in the top right and bottom right part of the network respectively. In the right part of those two networks, before those oil blobs appears, the oil trapping is lower in (Figure 8 iii.) than in (Figure 8 iv.) which is correct from a qualitative point of view. The capillary fingering seen in (Figure 8 v. and vi.) is more satisfactory than for (Lenormand et al. 1988), because when the Ca decreases, the trapped oil increases.

The third series of comparison consists in varying the viscosity ratio at a fixed capillary number of 1. The injected phase is in black (Figure 9).

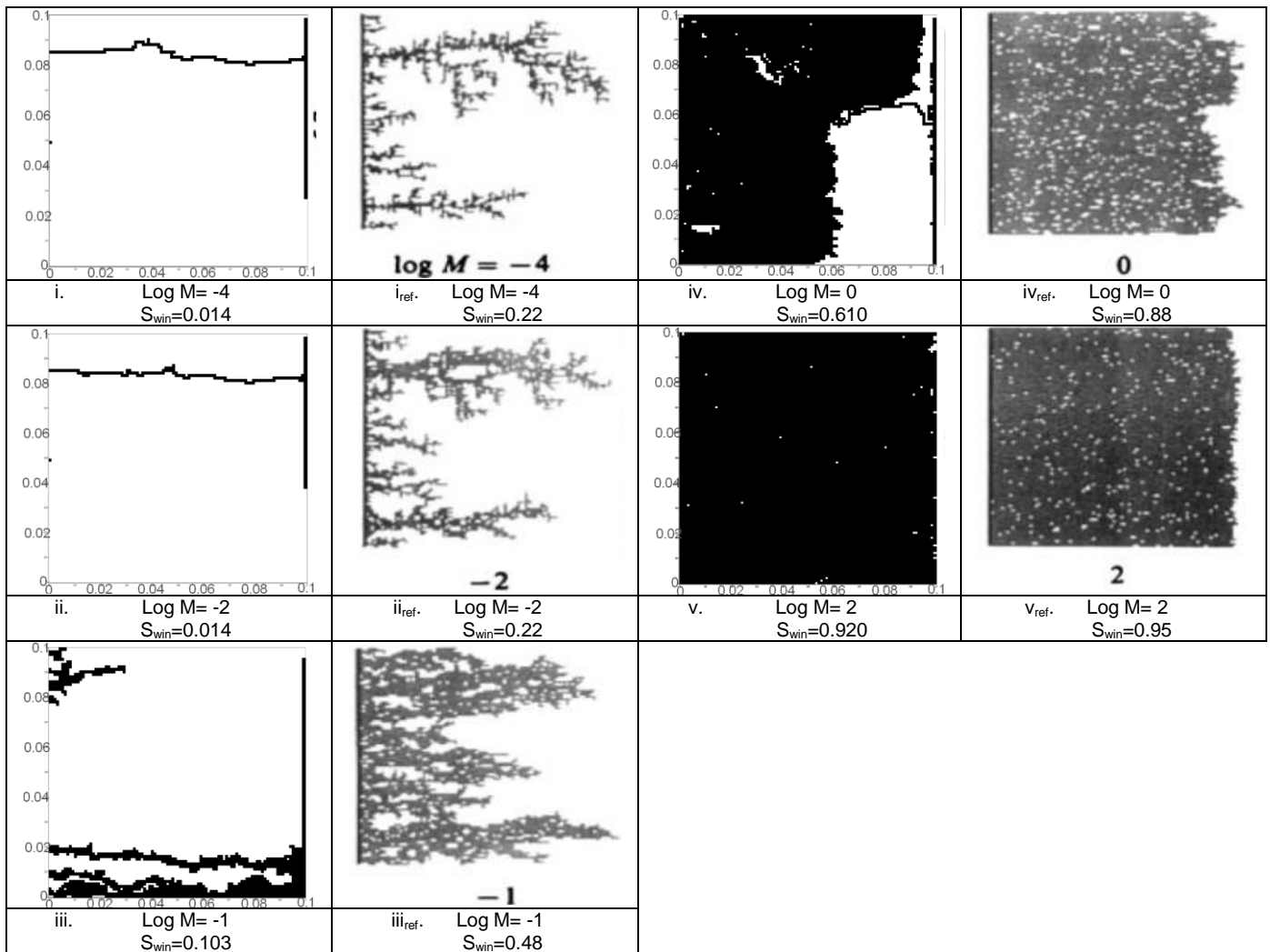
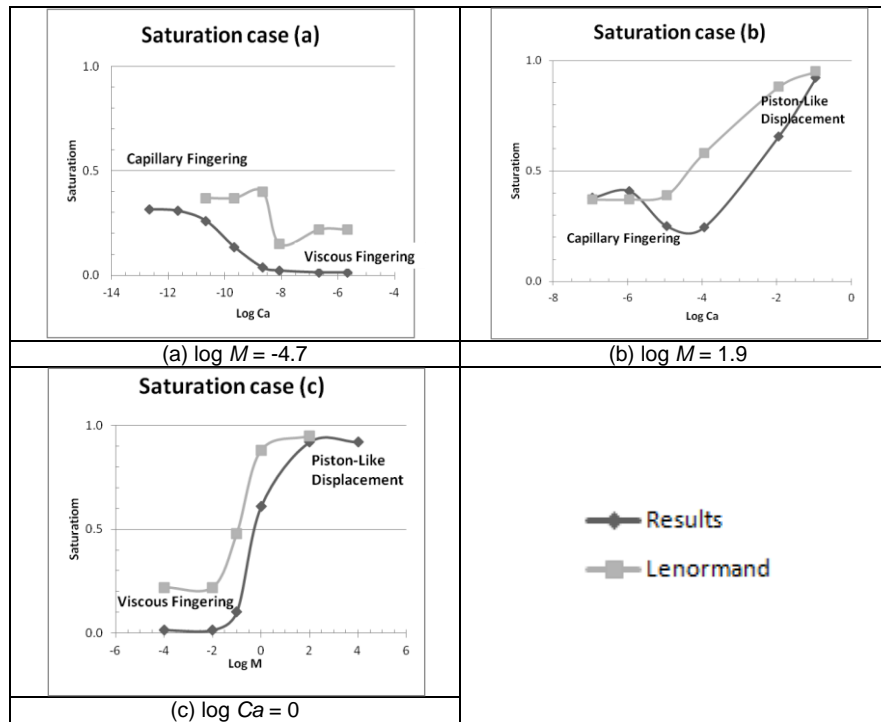


Figure 9: 100\*100 simulations while varying the viscosity ratio: (c)  $\log Ca = 0$ .

The first and third columns represent the results achieved and the second and fourth are the simulations by (Lenormand et al. 1988).

This series shows the transition between the viscous fingering and the piston-like displacement. At low viscosity ratios (Figure 9 i. and Figure 9 ii.), the viscous fingering that is achieved corresponds to the one that was seen in (Figure 6 i. and Figure 6 ii.). At high viscosity ratio (Figure 9 v.), the piston-like displacement happens exactly like for the Figure 8 i..

The injected fluid saturation profile analysis (Figure 10) allows quantifying with values the evolution between the patterns.



**Figure 10: 100\*100 simulations: plot of the injected fluid saturation when it has crossed the entire network; the points represent the results of the simulations and those by (Lenormand et al. 1988).**

For  $\log M = -4.7$  (case (a) Figure 10), the saturation has a maximum plateau at  $S_{winj} = 0.32$  and a minimum plateau at  $S_{winj} = 0.01$ . The higher plateau corresponds to capillary fingering and the smaller to viscous fingering. Unlike (Lenormand et al. 1988)'s simulations, the transition between them is smooth and the capillary fingering plateau is obtained for  $\log Ca < -10.7$ . This can also be explained by the existence in this code of flow in the wetting layers creating a faster flow towards the exit in the case of viscous fingering and therefore a very low injected fluid saturation.

The simulations ran with a constant  $\log M = 1.9$  (case (b) Figure 10), give a saturation curve that goes from a low plateau of  $S_{winj} = 0.38$  (capillary fingering) for a small Ca to a maximum of  $S_{winj} = 0.92$  (piston-like displacement) for higher Ca. The variation between the two plateaus is due to the way the code copes in some particular cases of flow to pores and throats of similar size. The flow will be favoured to go through to the ones closer to the exit of the network.

The third curve at  $\log Ca = 0$  (case (c) Figure 10) increases from  $S_{winj} = 0.01$  (viscous fingering) to  $S_{winj} = 0.92$  (piston-like displacement). The shape of the curve is exactly the same than in the (Lenormand et al. 1988) work and the difference in the values of the maximum is due to the fact that the networks used are not identically the same.



### 25\*25 network

The mean radius of the pores is equal to the mean radius of the throats  $r_0 = 0.56$  mm with a standard deviation of 0.7 for the throats and 0.2 for the pores. The same grid is used for all simulations. The same lines than for the 100\*100 network on the log-log M-Ca plot of simulations are run, plus a run of simulations at constant log Ca = -6.5

The saturation curves show the same shapes than for the 100\*100 network but as (Lenormand et al. 1988) explained, the position and the height of the plateau have changed due to the difference in the size of the network and pore size distribution.

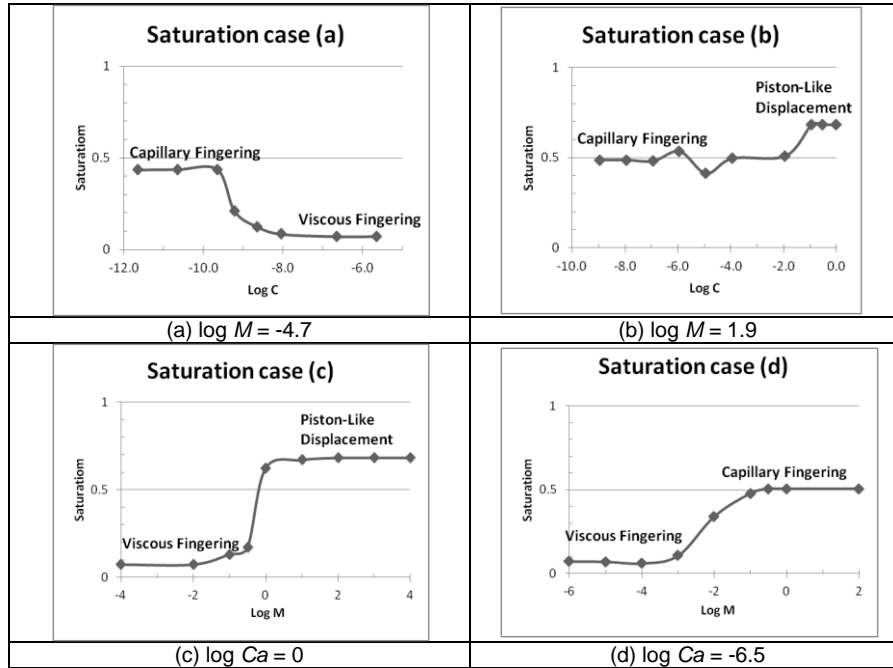


Figure 11: 25\*25 simulations: plot of the injected fluid saturation when it has crossed the entire network

In Figure 11, the different saturation plateaus can be seen clearly on the four different simulations run. The viscous fingering plateau is at a value of  $S_{winj} = 0.1$ , the capillary one is at around  $S_{winj} = 0.5$  and the piston-like displacement plateau is at  $S_{winj} = 0.7$ .

### Geometry of (Unsal et al. 2011)'s network

Another validation against a different set of laboratory experiments (Unsal et al. 2011) has been done. The porous medium is represented by a network of (120\*80) pores linked with neighbour pores by throats of a length of 40  $\mu\text{m}$ . The mean radius of the pores is equal to the mean radius of the throats  $r_0 = 50$   $\mu\text{m}$  with a standard deviation of 0.2 for the throats and 0.12 for the pores. The same grid is used for all simulations.

A comparison at two different mobility ratios is made:  $M < 1$  and  $M > 1$  are shown Figure 12 and Figure 13. The top row shows the ends of the laboratory experiments from (Unsal et al. 2011) when no further displacement was possible and beneath are the numerical simulations of the actual PNM. The complete fluid properties are listed Table 3 ( $M < 1$ ) and Table 4 ( $M > 1$ ) are done.

Table 3: Parameters used for the 120\*80 simulations at a constant  $M = 0.25$

Name	$\mu_w$ (Pa.s)	$\mu_o$ (Pa.s)	ift (N/m)	$q_w$ ( $\text{m}^3/\text{s}$ )	A ( $\text{m}^2$ )	$\cos(\theta)$	M	log M	Ca	log Ca
120by80_a1	1.00E-03	4.00E-03	2.00E-02	1.70E-10	9.52E-07	-1	0.25	-0.6	8.9E-06	-5.0
120by80_a2	1.00E-03	4.00E-03	2.00E-02	1.70E-09	9.52E-07	-1	0.25	-0.6	8.9E-05	-4.0

Table 4: Parameters used for the 120\*80 simulations at a constant  $M = 15$

Name	$\mu_w$ (Pa.s)	$\mu_o$ (Pa.s)	ift (N/m)	$q_w$ ( $\text{m}^3/\text{s}$ )	A ( $\text{m}^2$ )	$\cos(\theta)$	M	log M	Ca	log Ca
120by80_b1	1.50E-02	1.00E-03	3.00E-02	1.70E-12	9.52E-07	-1	15	1.2	8.9E-07	-6.0
120by80_b2	1.50E-02	1.00E-03	3.00E-02	1.70E-09	9.52E-07	-1	15	1.2	8.9E-04	-3.0

At  $M < 1$  (Figure 12), the numerical simulations show fair consistency with the experiments. On the left, the capillary effects are dominant; the fingers are typical of capillary fingering. On the right, the finger goes more directly towards the exit which is characteristic of the viscous effects taking over.

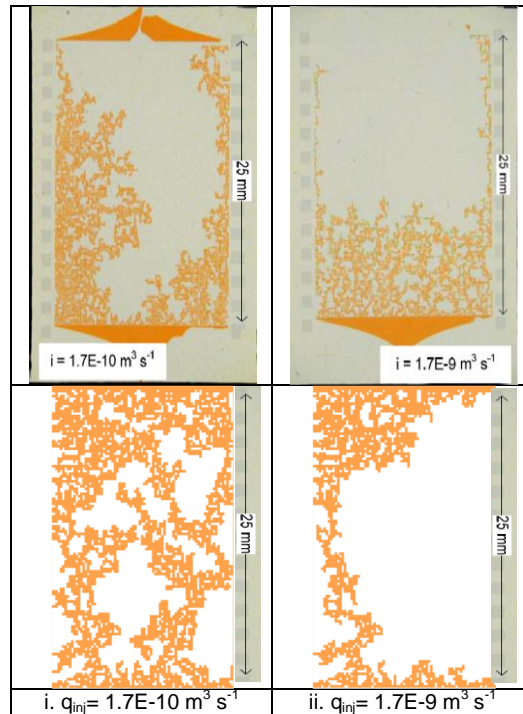


**Figure 12: 120\*80 simulations while varying the capillary number for  $M < 1$ . The first row is the experiments and the second row results achieved. Orange represents the liquid injected**

At  $M > 1$  (Figure 13), capillary fingering (on the left) and piston-like displacement (on the right) can be seen. The highest capillary number (on the right) gives the lower residual oil saturation and less trapped oil clusters. The numerical simulations compare well with the experiments.

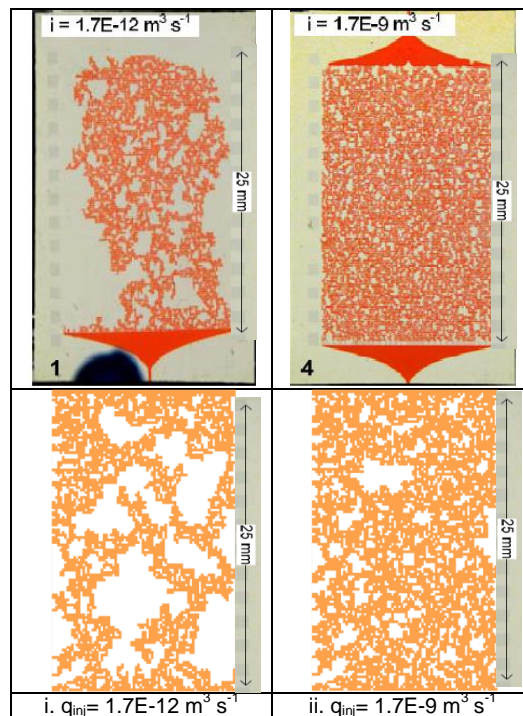


**Figure 13: 120\*80 simulations while varying the capillary number for  $M > 1$ . The first row is the experiments and the second row results achieved. Orange represents the liquid injected**

### Results with a 3D network

The possibility of simulating multiphase flow in 3D pore network models is also available. Simulations allowing checking of the consistency of the code are run on the carbonate C1 network provided by the Imperial College London Pore Scale Modelling department website. This network contains 4576 pores and 6921 throats. (<http://www3.imperial.ac.uk/earthscienceandengineering/research/perm/porescalemodelling/micro-ct%20images%20and%20networks/carbonate%20c1>).

A total of 12 simulations at different Ca numbers have been run at a constant  $\log M = -2$  and 14 simulations at  $\log M = -2$ . The summary of all simulations is shown Figure 14 which lists the residual injected saturation at different capillary numbers.

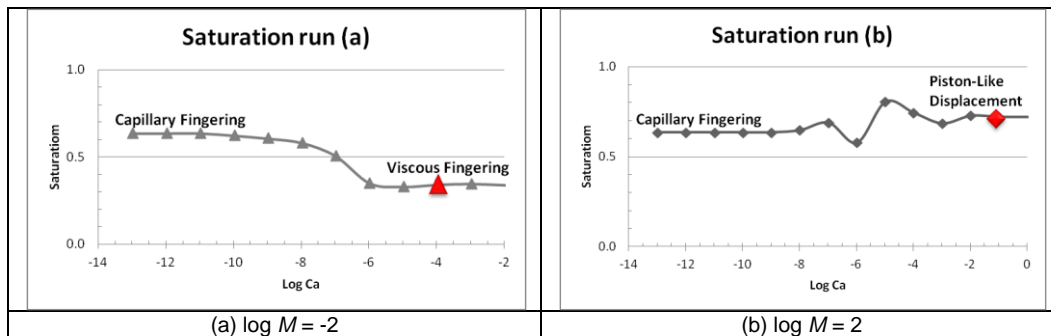


Figure 14: 3D network simulations: plot of the injected fluid saturation when it has crossed the entire network. In red are the cases where the pictures of the flow in the network are provided

The shapes of the curves are the ones expected: at  $\log M = -2$ , while increasing Ca, it goes from the capillary fingering to the viscous fingering flow pattern; at  $\log M = 2$ , while increasing Ca, it goes from the capillary fingering to the piston-like displacement flow pattern. The viscous fingering plateau is at a value of  $S_{winj} = 0.34$ , the capillary one is at around  $S_{winj} = 0.64$  and the piston-like displacement plateau is at  $S_{winj} = 0.75$ . Those shapes are consistent with the ones obtained by (Idowu and Blunt 2010).

In order to have a closer look at the fluid displacement profiles, visualizations from each mobility ratio are made. Figure 15 represents a case with  $M = -2$  obtained for the red triangle in Figure 14 (a). The injected water forms a finger through the oil.

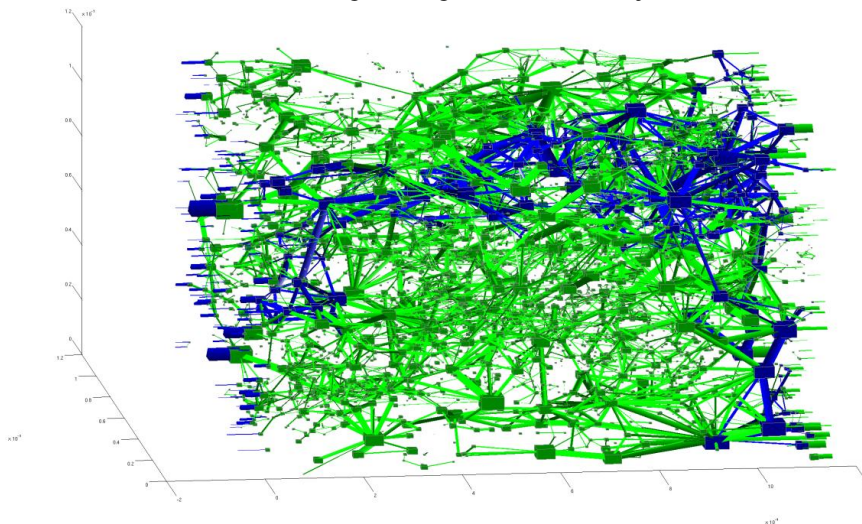
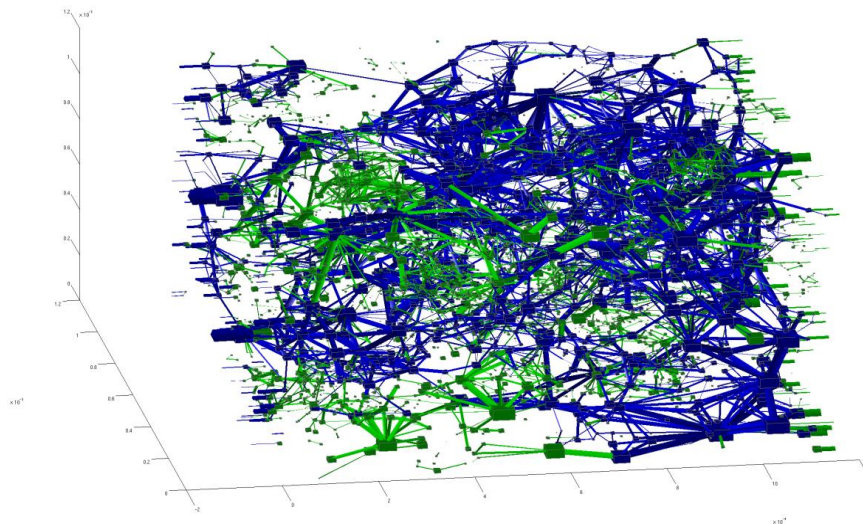


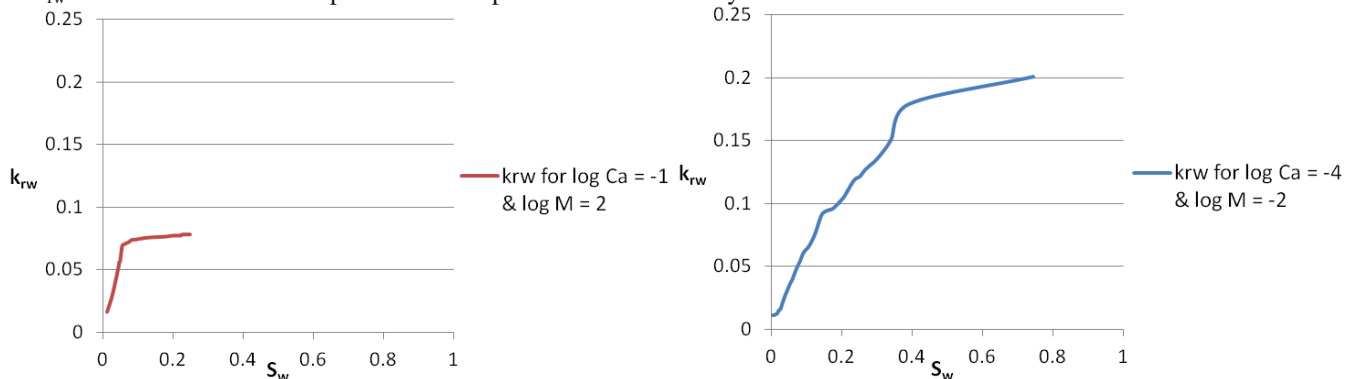
Figure 15: Viscous fingering in the carbonate C1 (provided by ICL) obtained at  $\log Ca = -4$  and  $\log M = -2$ . Blue corresponds to the water injected and green to the oil initially in place

Figure 16 represents a case for  $M = 2$ , obtained for the red losange in Figure 14 (b) Here the water is more distributed in the network and replaced more oil.



**Figure 16: Piston-like displacement in the carbonate C1 (provided by ICL) obtained at  $\log Ca = -1$  and  $\log M = 2$ . Blue corresponds to the water injected and green to the oil initially in place**

Water relative permeability ( $k_{rw}$ ) results were also extracted from those 3D experiments (Figure 17). On the left of Figure 17 the  $k_{rw}$  of Figure 15 is represented and on the right the  $k_{rw}$  of Figure 16. The water relative permeability for the viscous fingering displacement at its end point is smaller than for the piston-like displacement, a result which is expected. The shape of the  $k_{rw}$  obtained does not correspond to lab shapes and the reason why needs to be looked further in.



**Figure 17: Water relative permeability curves obtained for the viscous fingering (on the left) and the piston like-displacement (on the right) in the carbonate C1 (provided by ICL)**

## Discussion & Conclusion

This developed model gives a good basis towards the development of an efficient and accurate simulator of multiphase flow through pore networks. The improvement of the type of shapes the pores and throats can have, and the way the capillary pressure and the conductance get affected by that change, permit to say that the model is now more realistic. The existence of flow in the wetting layers of this dynamic pore network modeller goes also in that direction.

Meanwhile, work towards the improvement of the model can be achieved. An accurate simulation of the snap-off process should be done. The fact that the sizes of the wetting layers remain constant is also a point of improvement that needs to be looked in to. The code could be further developed so that it can deal with the presence of three phases in the network. The simulator is also able to deal with 3-D networks: checking the validity of the model with 3D cores would also be a quality testing job that could be done.

The validation of the work against others, especially laboratory experiments, provides an indication that the current model is able to capture the fundamental basics of two-phase flow. The fact that the agreement is fair and not perfect implies that the code still needs further improvement. It may be possible to use it to predict the phase saturations and relative permeabilities of cores and thus might prevent the usage of costly and time consuming real core analysis.

## Nomenclature

$A$	= cross-sectional area, $m^2$ .	$P_c$	= (threshold) capillary pressure, $Pa$ .
$A_w$	= cross-sectional area occupied by wetting fluid, $m^2$ .	$q$	= rate, $m^3/s$ .
$Ca$	= capillary number, <i>dimensionless</i> .	$r$	= radius, $m$ .



$G$ =	shape factor, <i>dimensionless</i> .	$\alpha$ =	half corner angle, <i>degrees</i> .
$h_c$ =	conductance, <i>S</i> .	$\theta$ =	contact angle, <i>degrees</i> .
$k$ =	constant, <i>dimensionless</i> .	$\mu$ =	viscosity, <i>Pa.s</i> .
$k_r$ =	relative permeability, <i>m<sup>2</sup></i> .	$\Sigma$ =	cross-sectional area of the sample
$M$ =	viscosity ratio, <i>dimensionless</i> .	$\sigma$ =	interfacial tension, <i>N/m</i> .
$P$ =	perimeter length of the shape, <i>m</i> .		

### Subscripts

$i_n$ =	injection	$s$ =	snap-off
$o$ =	oil (non-wetting fluid)	$t$ =	throat
$p$ =	pore	$w$ =	water (wetting fluid)

### Reference

- Constantinides, G.N. and Payatakes, A.C.: "A Theoretical Model of Collision and Coalescence of Ganglia in Porous Media" *Journal of Colloid and Interface Science* (1991) **141**, 486-504.
- Fatt, I.: "The Network Model of Porous Media I, II and III" *SPE 574, Trans. AIME* (1956) **107**, 144-181.
- Hammond, P.S. and Unsal, E.: "A Dynamic Pore Network Model for Oil Displacement by Wettability-Altering Surfactant Solution" *Transport in Porous Media* (2012) **92**, 789-817.
- Hughes, R.G. and Blunt, M.J.: "Pore Scale Modeling of Rate Effects in Imbibition" *Transport in Porous Media* (2000) **40**, 295-322.
- Idowu, N.A. and Blunt, M.J.: "Pore-Scale Modelling of Rate Effects in Waterflooding" *Transport in Porous Media* (2010) **83**, 151-169.
- Joekar-Niasar, V., Hassanizadeh, S.M. and Dahle, H.K.: "Non-equilibrium effects in capillarity and interfacial area in two-phase flow: dynamic pore-network modelling" *Journal of Fluid Mechanics* (2010) **655**, 38-71.
- Koplik, J. and Lasseter, T.J.: "Two-Phase Flow in Random Network Models of Porous Media" *Chem. Engng Commun.* (1985) **26**, 285-295.
- Kwon, B.S. and Pickett, G.R.: "A New Pore Structure Model and Pore Structure Interrelationships" *16th Annual Logging Symposium* (1975) 1-14.
- Lenormand, R. and Zarcone, C.: "Role of Roughness and Edges during Imbibition in Square Capillaries" paper SPE 13264 presented at the 59th Annual Technical Conference and Exhibition of the SPE of AIME, held in Houston, Texas, Sept., 16-19, 1984.
- Lenormand, R., Zarcone, C. and Touboul, E.: "Numerical Models and Experiments on Immiscible Displacements in Porous Media" *Journal of Fluid Mechanics* (1988) **189**, 165-187.
- Mason, G. and Morrow, N.R.: "Capillary behaviour of a perfectly wetting liquid in irregular triangular tubes" *Journal of Colloid and Interface Science* (1991) **141**, 262-274.
- Nguyen, V.H., Sheppard, A.P., Knackstedt, M.A. and Pinczewski, V.W.: "A Dynamic Network Model for Imbibition" paper SPE 90365 presented at the 2004 SPE International Petroleum Conference, Mexico, 8-9 Nov.
- Nguyen, V.H., Sheppard, A.P., Knackstedt, M.A. and Pinczewski, V.W.: "The Effects of Displacement Rate and Wettability on Imbibition Relative Permeabilities" paper SPE 95953 proceedings of the 2005 SPE Annual Technical Conference and Exhibition, Texas, 9-12 Oct.
- Øren, P.E. Bakke S. and Arntzen, O.J.: "Extending Predictive Capabilities to Network Models" paper SPE 38880 presented at the SPE Annual Technical Conference & Exhibition held in San Antonio, U.S.A., 5-8 October, 1997.
- Patzek, T.W.: "Verification of a Complete Pore Network Simulator of Drainage and Imbibition" paper SPE 71310 presented at the SPE/DOE Improved Oil Recovery Symposium, Tulsa, Oklahoma, 3-5 April, 2000
- Pickell, J.J., Swanson, B.F. and Hickmann, W.B.: "Application of Air-Mercury and Oil-Air Capillary Pressure Data in the Study of Pore Structure and Fluid Distribution" *SPE Journal* (1966) **6**, 55-61.
- Purcell, W.R.: "Capillary Pressures- Their Measurement Using Mercury and the Calculation of Permeability Therefrom" *Journal of Petroleum Technology* (1949) **1**, 39-48.
- Singhal, A.K. and Somerton, W.H.: "Two-phase Flow Through a Non-Circular Capillary at Low Reynolds Numbers" *Journal of Canadian Petroleum Technology* (1970) **9**, 197-198.
- Tuller, M., Or, D. and Dudley, L.M.: "Adsorption and capillary condensation in porous media: Liquid retention and interfacial configurations in angular pores" *Water Resources Research* (1999) **35** (7), 1949-1964.
- Unsal, E., Hammond, P.S. and Schneider, M.: "Effects of Surfactant on Wettability and Oil Recovery in a Pore Network Model" proceedings of the 16th European Symposium on Improved Oil Recovery, Cambridge, UK, 12-14 Apr. 2011.
- Valvatne, P.H., *Predictive Pore-Scale Modelling of Multiphase Flow*, PhD thesis, Imperial College London, 2004.
- Valvatne, P.H. and Blunt, M.J.: "Predictive Pore-Scale Network Modelling" paper SPE 84550 presented at the SPE Annual Technical Conference and Exhibition held in Denver, Colorado, U.S.A., 5 - 8 October 2003.

## Appendix A – Literature review and bibliography

### MILESTONES IN MULTIPHASE FLOW PORE SCALE NETWORK MODELLING

Journal Paper n°	Year	Title	Authors	Contribution
SPE 949039	1949	“Capillary Pressures- Their measurement using Mercury and the Calculation of Permeability Therefrom”	Purcell, W. R.	First to use the “bundle of tubes” as pore network consisting of parallel cylindrical tubes of various radii. First method of determining capillary pressures for porous media capillary pressure measurements using mercury found
SPE 574	1956	“The Network Model of Porous Media I, II and III”	Fatt, I.	First to use a network of tube as a real porous media rather than a bundle of tubes. Cross flow is for the first time allowed in a simulated pore network.
SPE Journal, 6	1966	“Application of Air-Mercury and Oil-Air Capillary Pressure Data in the Study of Pore Structure and Fluid Distribution”	Pickell, J.J. Swanson, B.F. Hickmann, W.B.	First to describe the snap-off process and to realise the importance of pore geometry by considering pores with angular cross-section.
J. Can. Petr. Tech., 9	1970	“Two-phase Flow Through a Non-Circular Capillary at Low Reynolds Numbers”	Singhal, A. K. Somerton, W. H.	First to use non-circular capillaries in simulation which is a better representation of the very irregular and random pore shapes. They used triangular shapes to represent the pores.
16 <sup>th</sup> Annual Logging Symposium	1975	“A New Pore Structure Model and Pore Structure Interrelationships”	Kwon, B.S. Pickett, G. R.	First to use both rectangular and triangular pore networks.
J. Fluid Mech., 135	1983	“Mechanisms of the Displacement of One Fluid by Another in a Network of Capillary Ducts”	Lenormand, R. Zarcone, C. Sarr, A.	This paper shows that the Laplace Law linking the capillary pressure to the interface curvature describes accurately enough the different flow mechanisms (piston-like displacement, snap-off, imbibition 1 and imbibition 2). It also shows that imbibition is controlled by the competition between different types of displacement mechanism.
SPE 13264	1984	“Role of Roughness and Edges during Imbibition in Square Capillaries”	Lenormand, R. Zarcone, C.	First to present the bond percolation, the compact cluster growth and the flat front advance type of flows.
Chem. Engng Commun., 26	1985	“Two-Phase Flow in Random Network Models of Porous Media”	Koplik, J. Lasseter, T. J.	Idea of modelling the porous medium by a network of randomly sized pores joined by randomly sized throats. Used the percolation theory to describe multiphase flow properties. They track the oil/water interface in detail.
J. Fluid Mech., 189	1988	“Numerical Models and Experiments on Immiscible Displacements in Porous Media”	Lenormand, R. Zarcone, C.	First to demonstrate the existence of three basic domains (capillary fingering, viscous fingering and stable displacement)
J. Colloid Interface Sci., 141	1991	“Capillary behaviour of a perfectly wetting liquid in irregular triangular tubes”	Mason G. Morrow N.R.	Introduction of the shape factor $G = A/P^2$ , as the voxel representation (for circular, triangular and rectangular shapes), where A is the cross-sectional area and P the perimeter length
J. Colloid Interface Sci., 141	1991	“A Theoretical Model of Collision and Coalescence of Ganglia in Porous Media”	Constantinides G.N. Payatakes A.C.	Included ganglia dynamics (ganglia is the blobs of trapped non-wetting phase)
SPE 39658	1998	“A Dynamic Pore-Scale Model of Imbibition”	Mogensen, K. Stenby, E.	This paper shows the sensitivity of residual oil saturation to contact angle, flow rate and aspect ratio using a dynamic network model of waterflooding.
SPE 38880	1998	“Extending Predictive Capabilities to Network Models”	Øren, P.-E. Bakke, S. Arntzen, O. J.	Gives the relationship giving the area occupied by the wetting fluid in corners of noncircular pores. Uses 2-D thin section to reconstruct a 3-D pore network model.
Water Resources Research, 35	1999	“Adsorption and capillary condensation in porous media: Liquid retention and interfacial configurations in angular pores”	Tuller, M. Or, D. Dudley, L.M.	Developed a model that accounts for wetting phase in corners and true film adsorption in very narrow regions
Transport in Porous Media, 40	2000	“Pore Scale Modeling of Rate Effects in Imbibition”	Hughes, R.G. Blunt, M. J.	Two flow regimes (ramified cluster growth and dendritic frontal advance) are described for the first time.
SPE 71310	2001	“Verification of a Complete Pore Network Simulator of Drainage and Imbibition”	Patzek, T. W.	It comes up with new hydraulic conductance correlations.
SPE 90365	2004	“A Dynamic Network Model for Imbibition”	Nguyen, V. H. Sheppard, A. P. Knackstedt, M. A. Pinczewski, V. W.	First to show the effect of displacement rate on imbibition patterns, relative permeabilities and residual saturations.
J. Fluid Mech., 655	2010	“Non-equilibrium effects in capillarity and interfacial area in two-phase flow: dynamic pore-network modelling”	Joekar-Niasar V. Hassanizadeh S.M. Dahle H.K.	Included the effect of the interfacial area at the oil/water interphase.

- 1 Blunt, M.J.: "Flow in Porous Media -- Pore-Network Models and Multiphase Flow" *Current Opinion in Colloid & Interface Science* (2001) **6**, 197-207.
- 2 Blunt, M.J., Jackson, M.D., Piri, M. and Valvatne, P.H.: "Detailed physics, predictive capabilities and macroscopic consequences for pore-network models of multiphase flow" *Advances in Water Resources* (2002) **25**, 1069.
- 3 Constantinides, G.N. and Payatakes, A.C.: "A Theoretical Model of Collision and Coalescence of Ganglia in Porous Media" *Journal of Colloid and Interface Science* (1991) **141**.
- 4 Dong, M. and Chatzis, I.: "The Imbibition and Flow of a Wetting Liquid along the Corners of a Square Capillary Tube." *Journal of Colloid and Interface Science* (1995) **172**, 278-288.
- 5 Fatt, I.: "The Network Model of Porous Media I, II and III" *SPE 574, Trans. AIME* (1956) **107**.
- 6 Gassmann, F.: "Elastic Waves through a Packing of Spheres" *Geophysics* (1951) **16**, 673-685.
- 7 Hammond, P.S. and Unsal, E.: "A Dynamic Pore Network Model for Oil Displacement by Wettability-Altering Surfactant Solution" *Transport in Porous Media* (2012) **92**, 789-817.
- 8 Hughes, R.G. and Blunt, M.J.: "Pore Scale Modeling of Rate Effects in Imbibition" *Transport in Porous Media* (2000) **40**, 295-322.
- 9 Idowu, N.A. and Blunt, M.J.: "Pore-Scale Modelling of Rate Effects in Waterflooding" *Transport in Porous Media* (2010) **83**, 151-169.
- 10 Jackson, M.D., Valvatne, P.H. and Blunt, M.J.: "Prediction of wettability variation and its impact on flow using pore-to reservoir-scale simulations" *Journal of Petroleum Science and Engineering* (2002) **39**, 231.
- 11 Joekar-Niasar, V., Hassanizadeh, S.M. and Dahle, H.K.: "Non-equilibrium effects in capillarity and interfacial area in two-phase flow: dynamic pore-network modelling" *Journal of Fluid Mechanics* (2010) **655**, 38-71.
- 12 Koplik, J. and Lasseter, T.J.: "Two-Phase Flow in Random Network Models of Porous Media" *Chem. Engng Commun.* (1985) **26**, 285-295.
- 13 Kwon, B.S. and Pickett, G.R.: "A New Pore Structure Model and Pore Structure Interrelationships" *16th Annual Logging Symposium* (1975) 1-14.
- 14 Legait, B.: "Laminar Flow of Two Phases through a Capillary Tube with Variable Square Cross-Section" *Journal of Colloid and Interface Science* (1983) **96**, 1.
- 15 Lenormand, R., Zarcone, C. and Sarr, A.: "Mechanisms of the Displacement of One Fluid by Another in a Network of Capillary Ducts" *Journal of Fluid Mechanics* (1983) **135**, 337-353.
- 16 Lenormand, R. and Zarcone, C.: "Role of Roughness and Edges during Imbibition in Square Capillaries" *SPE 13264* (1984).
- 17 Lenormand, R., Zarcone, C. and Touboul, E.: "Numerical Models and Experiments on Immiscible Displacements in Porous Media" *Journal of Fluid Mechanics* (1988) **189**, 165-187.
- 18 Mason, G. and Morrow, N.R.: "Capillary behaviour of a perfectly wetting liquid in irregular triangular tubes" *Journal of Colloid and Interface Science* (1991) **141**.
- 19 Mogensen, K. and Stenby, E.: "A Dynamic Pore-Scale Model of Imbibition" *SPE 39658*, (1998).
- 20 Nguyen, V.H., Sheppard, A.P., Knackstedt, M.A. and Pinczewski, V.W.: "A Dynamic Network Model for Imbibition" paper SPE 90365 presented at the 2004 SPE International Petroleum Conference, Mexico, 8-9 Nov.
- 21 Nguyen, V.H., Sheppard, A.P., Knackstedt, M.A. and Pinczewski, V.W.: "The Effects of Displacement Rate and Wettability on Imbibition Relative Permeabilities" paper SPE 95953 proceedings of the 2005 SPE Annual Technical Conference and Exhibition, Texas, 9-12 Oct..
- 22 Øren, P.E. and Bakke, S.: "Reconstruction of Berea sandstone and pore-scale modelling of wettability effects" *Journal of Petroleum Science and Engineering* (2003) **39**, 177.
- 23 Øren, P.E. Bakke S. and Arntzen, O.J.: "Extending Predictive Capabilities to Network Models" *SPE 38880* (1998) 324-326.
- 24 Patzek, T.W.: "Verification of a Complete Pore Network Simulator of Drainage and Imbibition" *SPE 71310* (2001) 144.
- 25 Pickell, J.J., Swanson, B.F. and Hickmann, W.B.: "Application of Air-Mercury and Oil-Air Capillary Pressure Data in the Study of Pore Structure and Fluid Distribution" *SPE Journal* (1966) **6**, 55-61.
- 26 Purcell, W.R.: "Capillary Pressures- Their measurement using Mercury and the Calculation of Permeability Therefrom" *Journal of Petroleum Technology* (1949).
- 27 Ransohoff, T.C. and Radke, C.J.: "Laminar flow of a wetting liquid along the corners of a predominantly gas-occupied noncircular pore" *Journal of Colloid and Interface Science* (1988) **121**, 392.
- 28 Singhal, A.K. and Somerton, W.H.: "Two-phase Flow through a Non-Circular Capillary at Low Reynolds Numbers" *Journal of Canadian Petroleum Technology* (1970) **9**, 197-198.
- 29 Tuller, M., Or, D. and Dudley, L.M.: "Adsorption and capillary condensation in porous media: Liquid retention and interfacial configurations in angular pores" *Water Resources Research* (1999) **35** (7), 1949-1964.

- 
- 30 Unsal, E., Hammond, P.S. and Schneider, M.: "Effects of Surfactant on Wettability and Oil Recovery in a Pore Network Model". proceedings of the 16th European Symposium on Improved Oil Recovery, Cambridge, UK, 12-14 Apr. 2011.
- 31 Valvatne, P.H., *Predictive Pore-Scale Modelling of Multiphase Flow*, PhD thesis, Imperial College London, 2004.
- 32 Valvatne, P.H. and Blunt, M.J.: "Predictive Pore-Scale Network Modelling" *SPE 84550*, (2003).



---

**Jour. Pet. Tech. (Feb. 1949)**

**Capillary Pressures- Their measurement using Mercury and the Calculation of Permeability Therefrom**

Authors: Purcell, W. R.

Contribution to the understanding of pore network modelling:

Utilisation of the “bundle of tubes” as pore network consisting of parallel cylindrical tubes of various radii. It is a simplified and false model compared to reality but it allows calculating easily capillary pressure curves and permeability.

Objectives of the paper:

Describe a method and procedure for determining capillary pressure curves for porous media.

Methodology used:

An apparatus is used for determining mercury capillary pressures.

Conclusion reached:

A method of determining capillary pressures for porous media capillary pressure measurements using mercury has been determined. The work pointed pore structure research in the direction of bundles of capillary tubes as models of pore systems.

Comments:

The bundle of tubes model is a one dimensional pore system without pore interconnections, while actual rocks have complicated and irregular interconnections.

---

**Geophysics, 16, 673-685 (1951)****Elastic Waves Through a Packing of Spheres**

Authors: Gassmann, F.

Contribution to the understanding of pore network modelling:

This paper presents a pore network as a close packing of equal spheres.

Objective of the paper:

The elasticity of a hexagonal close packing of equal spheres is treated.

Methodology used:

It uses the results of a previous paper by the author (Gassmann, 1951) for the elasticity of homogeneous isotropic or anisotropic porous solids.

Conclusion reached:

The results obtained show some typical effects such as anisotropy, inhomogeneity, and a 90° angle of emergence.

Comments:

Spherical packings are useful for studying stress-strain relations in porous media, but can only represent granular rocks with ideal sorting. They present pore space configurations which complicate the calculation of electrical or fluid flow properties.

---

**SPE 574, Trans. AIME, 107 (1956)**

### **The Network Model of Porous Media I, II and III**

Authors: Fatt, I.

Contribution to the understanding of pore network modelling:

This paper proposes a network of tube as a real porous media rather than a bundle of tubes. Cross flow is for the first time allowed in a simulated pore network.

Objective of the paper:

Show the difference between the true and calculated pore size distributions when the capillary pressure curve is used to obtain pore size distribution for porous media.

Methodology used:

Two-dimensional regular network of tubes of randomly distributed radii is used as a model.

Conclusion reached:

It shows that the bundle of tubes is generally inappropriate to interpret the capillary pressure curve.

It also points out that while the multiphase flow properties are a function of both network form and pore size distribution, it is the network structure which determines the overall behaviour of real systems.

Comments:

Some assumptions are not realistic in representing real rocks.

---

**SPE Journal, 6, 55-61 (1966)**

**Application of Air-Mercury and Oil-Air Capillary Pressure Data in the Study of Pore Structure and Fluid Distribution**

Authors: Pickell, J.J.; Swanson, B.F.; Hickmann, W.B.

Contribution to the understanding of pore network modelling:

First to describe the snap-off process and to realise the importance of pore geometry by considering pores with angular cross-section.

Objectives of the paper:

Investigate the mechanism of capillary trapping and assess its importance in laboratory measurements of residual oil saturation.

Methodology used:

Used the air-mercury and oil-air capillary pressure data measurements.

Conclusion reached:

Fluid distribution in a porous medium is a function of pore size distribution, pore configurations, interfacial properties and previous saturation history.

Residual non-wetting phase saturations are a function of both pore geometry and initial saturation.

Comments:

The air-mercury process has some defaults: it is not always accurate and mercury does not always act as a strongly non-wetting liquid.

---

**J. Can. Petr. Tech., 9, 197-198 (1970)**

**Two-phase Flow Through a Non-Circular Capillary at Low Reynolds Numbers**

Authors: Singhal, A. K.; Somerton, W. H.

Contribution to the understanding of pore network modelling:

They were the first to use non-circular capillaries which is a better representation of the very irregular and random pore shapes. They used triangular shapes to represent the pores.

Objectives of the paper:

Explore the problems of two phase flow in non-circular capillaries at low Reynolds numbers.

Methodology used:

Expressions are derived for the shapes of fluid-fluid interfaces in terms of contact angles and fluid saturations. Velocity distributions within the channel are obtained by analytical and numerical variational procedures.

Conclusion reached:

Contact angles and viscosity ratios influence two-phase flow through porous media.

The displacement flow regime apart from imbibition and slug flow regime give extra resistances which tend to lower relative permeabilities.

Comments:

The results are inferred and no experimental evidence is present to confirm the hypotheses concerning the flow characteristics from duct flows.

---

**16<sup>th</sup> Annual Logging Symposium, 1-14 (1975)****A New Pore Structure Model and Pore Structure Interrelationships**

Authors: Kwon, B.S.; Pickett, G. R.

Contribution to the understanding of pore network modelling:

Utilisation of rectangular and triangular pore networks.

Objectives of the paper:

Improve the knowledge of rock properties associated with pore structure and to achieve a better understanding of the relations among such properties.

Methodology used:

Angular models were chosen to represent individual pores. Two basic pore models, triangular (equilateral) and rectangular (square) were employed.

Physical properties of porous rock and their interrelationships are investigated by derivation of a mathematical pore structure model and empirical study.

Conclusion reached:

The pore structure model, while still requiring further research, represents a potentially valuable tool in investigating interrelationships (for example estimating permeability from well logs) of rock properties of economic significance.

Comments:

It seems that the influence of the shape on fluid behaviour is not incorporated in the analysis.

**J. Fluid Mech., 135, 337-353 (1983)**

## **Mechanisms of the Displacement of One Fluid by Another in a Network of Capillary Ducts**

Authors: Lenormand, R.; Zarcone, C.; Sarr, A.

### Contribution to the understanding of pore network modelling:

This paper shows that the Laplace Law linking the capillary pressure to the interface curvature ( $P_c = \sigma (1/r_1 + 1/r_2)$ ) describes accurately enough the different flow mechanisms (piston-like displacement, snap-off, imbibition 1 and imbibition 2). It also shows that imbibition is controlled by the competition between different types of displacement mechanism.

### Objectives of the paper:

Study the mechanisms of displacement of one fluid by another in an etched network.

### Methodology used:

They used the technique developed by Bonnet & Lenormand (1977) which is the moulding technique using transparent polyester resin and photographically etched mould.

### Conclusion reached:

Oil and water are simultaneously present in a duct with the wetting fluid staying in the corners of the cross-section.

For "piston-type" motion: the non-wetting fluid enters the duct filled with wetting fluid only if the capillary pressure is equal to or greater than the "threshold pressure" ( $P_p = 2\sigma (1/x + 1/y)$ )

"Snap-off" occurs at a the snap-off pressure of  $P_s = 2\sigma/x$  (if  $x < y$ ) or  $P_s = 2\sigma/y$  (if  $y < x$ )

Imbibition I1 (the non-wetting fluid is in one duct): When there is an increase in the wetting fluid pressure, the capillary pressure decreases and instability appears when the meniscus no longer touches the wall.

Imbibition I2 (non-wetting fluid in two adjacent ducts): There is a collapse for a pressure  $P_{I2} = 2\sigma (0.15/x + 1/y)$

### Comments:

The size of the network used is limited to emphasize the physical mechanism. It is not a real porous medium

**Journal of Colloid and Interface Science, 96, 1 (1983)**

**Laminar Flow of Two Phases through a Capillary Tube with Variable Square Cross-Section**

Authors: Legait B.

Contribution to the understanding of pore network modelling:

Capillary pressure expression for square capillaries.

Objective of the paper:

Study the effect of viscosity on the droplets flow in a capillary tube with variable cross-section.

Methodology used:

The angularity of the channels in a porous medium and the variation in their cross-section were schematized by a constricted capillary tube of square cross-section.

Conclusion reached:

The greater the droplet viscosity the more easily the droplet flows through the capillary tube whatever the boundary conditions. It is also true in a pore doublet due to the internal flow in the droplet.

Capillary pressure in square capillaries:

$$P_c = \frac{\gamma}{r} \left( \frac{\theta + \cos^2(\theta) - \pi/4 - \sin(\theta)\cos(\theta)}{\cos(\theta) - \sqrt{\pi/4 - \theta + \sin(\theta)\cos(\theta)}} \right)$$

Comments:

Some features of porous media are not taken into account by the simple tube shape described in the present paper (roughness, connectivity).



## SPE 13264 (1984)

### Role of Roughness and Edges during Imbibition in Square Capillaries

Authors: Lenormand, R.; Zarcone, C.

#### Contribution to the understanding of pore network modelling:

This paper helps to understand the flow behaviour during imbibition in a rough and edgy pore network. It presents also the bond percolation, the compact cluster growth and the flat front advance type of flows.

#### Objectives of the paper:

- 1) This paper describes all the physical mechanisms observed during imbibition at different flow rates in an etched network, and, taking into account these observations, especially the film flow, to build a general but realistic model.
- 2) Show that the spatial distribution of fluids is linked to the following parameters:
  - The geometry of the pores and throats;
  - Fluid properties;
  - Roughness of the ducts;
  - Capillary number (CA).

#### Methodology used:

For imbibition experiments a 42,000 duct network with seven classes of width roughly distributed as a log-normal law was used. The experiments are run at different capillary number  $CA$ , the ratio between viscous and capillary forces:  $CA = \frac{Q \mu}{L x \gamma}$

In this equation,  $\mu$  is the wetting fluid viscosity,  $\gamma$  the surface tension between the fluids,  $Q$  the total flow rate in the network and  $L$  the width of the network.

#### Conclusion reached:

This study points out the important role of the flow by roughness and corners of the ducts during imbibitions in an etched network:

- The basic *or* “reference” mechanism is a flat frontal drive without trapping of the nonwetting phase (value  $CA > 10^{-4}$ ) However, the shape of the interface is only due to a specific mechanism and not to a viscous pressure drop.
- When the capillary number decreases, the flow by roughness and corners “has enough time” to take place and acts like a “suction” on the interface and consequently the capillary pressure increases along the interface between the fluids, the pressure inside the bulk wetting phase remaining constant.
- The value of the capillary pressure leads to selection for the mechanisms of meniscus displacement and the shape of the front is a consequence of the kind and the fraction of allowed mechanisms.
- *Classical bond percolation:* we are cutting bonds in the network until the nonwetting phase becomes discontinuous.
- *Nucleation cluster growth:* In the absence of lateral edges in the network, the only way for Imbibition to take place is snap-off, but the capillary pressure is very low and when two adjacent ducts are filled the I2 displacement takes place instantaneously and tills the pore and the two other ducts the hatched cluster will grow and invade the whole latticed theory that this critical fraction is not a percolation threshold but tends to zero as the network size increases..

#### Comments:

The paper deals with flow through an etched network and not a real porous medium, so even if they can be comparable they are not exactly the same. They also use the hydraulic-diameter approximation to solve the corner flow problem, a procedure that is in error for the laminar flow regime.

---

**Chem. Engng Commun., 26, 285-295 (1985)**

**Two-Phase Flow in Random Network Models of Porous Media**

Authors: Koplik, J.; Lasseter, T. J.

Contribution to the understanding of pore network modelling:

Idea of modelling the porous medium by a network of randomly sized pores joined by randomly sized throats. Uses the percolation theory to describe multiphase flow properties.

Objectives of the paper:

Explore how the microscopic geometry of a pore space affects the macroscopic characteristics of fluid flow in porous media.

Methodology used:

Modelling of a porous medium by a network of randomly sized pores joined by randomly sized throats.

Conclusion reached:

The immiscible displacement process is affected by the external and boundary conditions, the fluid parameters and the geometry of the porous medium.

Comments:

In the research the fluids have been assumed as being incompressible, immiscible, Newtonian and of equal viscosity. The flow in wetting layers has been neglected.

---

**J. Fluid Mech., 189, 165-187 (1988)**

## **Numerical Models and Experiments on Immiscible Displacements in Porous Media**

Authors: Lenormand, R.; Zarcone, C.

### Contribution to the understanding of pore network modelling:

Demonstrates the existence of three basic domains (capillary fingering, viscous fingering and stable displacement)

### Objectives of the paper:

Verification of the notion of phase-diagram in the case of a two-dimensional porous medium made of interconnected capillaries.

### Methodology used:

Injection of a non-wetting fluid into a two-dimensional porous medium made of interconnected capillaries.

Use of network simulators (100 x 100 and 25 x 25 pores) based on the physical rules of the displacement at the pore scale.

Then to compare, series of experiments performed in transparent etched networks are done.

### Conclusion reached:

The reproducibility of the 'numerical experiments' allows the study of parameters (such as the final saturation) that are difficult to obtain in physical experiments. In addition, numerical experiments can be performed when physical experiments are impossible because of technical limitations (pressure, time), which is the case for the series at  $\log Ca = 0$ .

The second point concerns the notion of the phase-diagram. Both simulations and experiments show the existence of three main regimes: stable displacement, viscous fingering and capillary fingering, which can be mapped on the phase diagram: the viscosity ratio-capillary number plane.

Each of these main regimes can be described by a statistical model: anti-DLA, DLA and invasion percolation.

### Comments:

The paper deals with flow through an etched network and not a real porous medium, so even if they can be comparable they are not exactly the same.

**J. Colloid Interface Sci., 121, 392 (1988)****Laminar flow of a wetting liquid along the corners of a predominantly gas-occupied noncircular pore**

Authors: Ransohoff, T.C.; Radke, C. J.

Contribution to the understanding of pore network modelling:

Creation of the concept of the dimensionless flow resistance in the corners of capillary tubes.

Objectives of the paper:

Study the effect of corner geometry and contact angle on laminar flow along the corners of noncircular pores.

Methodology used:

A two-dimensional hydrodynamic solution is shown for the flow of a wetting liquid at low Reynolds numbers along the corners of a gas-saturated noncircular pore.

Conclusion reached:

The dimensionless flow resistance ( $\beta = a^2 / \mu * v_z * -dp_1/dz$ ) where  $a$  is the radius of the gas-liquid interface circular arc,  $\mu$  is the fluid viscosity,  $v_z$  is the average velocity) increases with increasing half angle, degree of roundedness, surface shear viscosity and contact angle.

They also demonstrated that the error resulting from the use of the hydraulic-diameter approximation is on the order of 50% or higher.

Comments:

---

**J. Colloid Interface Sci., 141 (1991)****A Theoretical Model of Collision and Coalescence of Ganglia in Porous Media**

Authors: Constantinides, G.N.; Payatakes, A.C.

Contribution to the understanding of pore network modelling:

Included ganglia dynamics (ganglia is the blobs of trapped non-wetting phase)

Objectives of the paper:

Present a theoretical model of the process of collision and coalescence of a pair of mobilized ganglia in porous media, and investigate the conditions under which coalescence is prompt or difficult.

Methodology used:

The porous medium is modelled as a three-dimensional network of randomly sized unit cells of the constricted-tube type, pertaining to consolidated porous materials.

The problem of simultaneous flow of the two ganglia in the porous medium is solved using the network approach.

The details of the flow near and between the two colliding menisci are analyzed with a film drainage model, which takes into account the presence of the constraining pore wall, the wetting film which surrounds the ganglia by occupying roughness features on the pore wall, and the hydrodynamic interactions of the three liquid bodies.

Conclusion reached:

The probability of coalescence between pairs of moving ganglia depends mainly on wettability and less on neither the capillary number nor the viscosity ratio.

The probability of coalescence between pairs of moving ganglia decreases strongly as the values of contact angles increase

Comments:

The model developed does not cope well when the oil and water viscosities are too close to one another and approximations have been made in that case.

**J. Colloid Interface Sci., 141 (1991)****Capillary behaviour of a perfectly wetting liquid in irregular triangular tubes**

Authors: Mason, G.; Morrow, N.R.

Contribution to the understanding of pore network modelling:

Introduction of the shape factor  $G = A/P^2$ , as the voxel representation (for circular, triangular and rectangular shapes), where A is the cross-sectional area and P the perimeter length.

Objectives of the paper:

Derive the exact meniscus curvature of perfectly wetting liquids draining from pores of general triangular cross section.

Methodology used:

The method relies on equating the curvature of the arc menisci that always exist in the corners of the tube to the curvature of the main terminal meniscus (invading meniscus) in the tube. It is a method that was originally proposed by Mayer and Stowe (1965).

Conclusion reached:

There is hysteresis between drainage and imbibition and trapping of the non-wetting phase. The natural normalizing shape factor is shown to be  $A/P^2$  (where A is the triangle area and P its perimeter). Tubes with the same shape factor have the same capillary behaviour even though they are geometrically different. Systems with finite contact angle can be treated by a similar approach, but the analysis is more complicated.

Comments:

Systems with finite contact angle were not treated.

---

**Journal of Colloid and Interface Science, 172, 278-288 (1995)**

## **The Imbibition and Flow of a Wetting Liquid along the Corners of a Square Capillary Tube**

Authors: Dong, M.; Chatzis, I.

### Contribution to the understanding of pore network modelling:

First to report imbibition experiments in square capillary tubes of the type. Improved the theory predicting the imbibition rate of a wetting liquid in the corners of a square capillary tube occupied predominantly by the non-wetting gas phase.

### Objectives of the paper:

Study the dependence of imbibition rate on the surface tension and viscosity of the spreading liquid, to study the dependence of spreading rate on the wetting ability of the spreading fluid on the solid surface, and to investigate the effect of corner geometry on the spreading rate.

### Methodology used:

The dimensionless flow resistance in the corners of capillary tubes (Ransohoff and Radke, 1988) was applied to the imbibition of a wetting liquid in the corners of a square capillary tube occupied predominantly by non wetting air.

### Conclusion reached:

The imbibition rate decreases when the spreading fluid does not wet perfectly the tube wall since the cross section area available for the flow of the wetting fluid in the corners becomes smaller when the contact angle increases.

The velocity of imbibition depends on the fluid properties (surface tension, viscosity), the contact angle, and the geometry of the corner.

In their theory, the imbibition velocity is proportional to  $D^{0.5}$  where D is the tube size.

### Comments:

The free imbibition of wetting phase in porous media is not yet fully understood and they want to do more research on spreading of wetting liquid in single capillaries to do so.

**SPE 38880, 324-326 (1998)**

### **Extending Predictive Capabilities to Network Models**

Authors: Øren, P.-E.; Bakke, S.; Arntzen, O. J.

#### Contribution to the understanding of pore network modelling:

Utilisation of image analyses of 2D thin section sections to generate a reliable reconstruction of the complex rock-pore system in 3-D. Gives the relationship giving the area occupied by the wetting fluid in corners of noncircular pores

#### Objectives of the paper:

Compare the predicted transport properties for different sandstones with experimental data.

#### Methodology used:

Reconstruction of 3-D sandstone models giving a realistic description of the complex pore space observed in actual sandstones. The reconstructed pore space is transformed into a pore network which is used as input to a two-phase network model. The model simulates primary drainage and water injection based on a physical scenario for wettability changes at the pore level.

The conductance used to calculate the film rate is  $g = \frac{r_w^2 A}{C_w \mu}$ , where  $C_w$  is the Ransohoff and Radke dimensionless flow resistance factor which accounts for the reduced water conductivity close to the pore walls,  $A$  is the triangular cross-section,  $r_w = \gamma/P_c$  the radius of curvature of the filament set by the prevailing capillary pressure,  $P_c$ , and the interfacial tension,  $\gamma$  and  $\mu$  the fluid viscosity.

Pore bodies and throats are assumed to have a triangular cross-section with area  $A = r^2/4G$ . When water is present as AMs in the corners of a pore body or throat, the area occupied by the water is given by

$$A_w = r_w^2 \sum_{i=1}^3 \left[ \frac{\cos \theta \cos(\theta + \beta_i)}{\sin \beta_i} - \frac{\pi}{2} \left( 1 - \frac{\theta + \beta_i}{90} \right) \right]$$

where  $r_w = \gamma/P_c$  is the radius of curvature of the AMs

$\theta$  = contact angle

$\beta$  = corner half angle

#### Conclusion reached:

The reconstruction process gives realistic descriptions of the microstructure of real sandstones.

The permeabilities, formation factor and relative permeabilities of the reconstructed sandstones are in fair agreement with experimental measurements.

#### Comments:

The experiments have been made on a small number of samples so a larger group of petrographically and petrophysically heterogeneous rock samples should be further analyzed.



---

**SPE 39658 (1998)****A Dynamic Pore-Scale Model of Imbibition**

Authors: Mogensen, K.; Stenby, E.

Contribution to the understanding of pore network modelling:

This paper helps to understand the sensitivity of residual oil saturation to contact angle, flow rate and aspect ratio using a dynamic network model of waterflooding.

Objective of the paper:

It describes the sensitivity of the type of flow (piston-like and snap-off) and therefore residual oil, towards capillary number, contact angle and aspect ratio.

Methodology used:

Construction of a dynamic pore-scale 3-D network model of wide pore spaces which are connected by more narrow regions termed throats of imbibition. It is capable of calculating residual oil saturation for any given capillary number, viscosity ratio, contact angle and aspect ratio.

Conclusion reached:

The residual oil saturation depends on factors which influence the balance between snap-off (higher  $S_{or}$ ) and frontal displacement (lower  $S_{or}$ ).

The snap-off events are reduced by an increase of the contact angle.

$S_{or}$  reduces when CA increases.

The increase of the aspect ratio leads to a reduction of the snap-off time and so favour throat filling ahead of the connected front.

Comments:

Long range correlation in pore and throat sizes were not done due to CPU-time requirements so the gradual suppression of snap-off is at one order of magnitude of the capillary number.

**Water Resources Research, 35 (7), 1949-1964 (1999)**

**Adsorption and capillary condensation in porous media:  
Liquid retention and interfacial configurations in angular pores**

Authors: Tuller, M.; Or, D.; Dudley, L.M.

Contribution to the understanding of pore network modelling:

Developed a model that accounts for wetting phase in corners and true film adsorption in very narrow regions.

Objectives of the paper:

Propose a pore-scale liquid retention modelling approach based on two elements: (1) explicit consideration of the individual contributions of adsorptive and capillary forces to the matric potential based on the augmented Young-Laplace (AYL) equation, and (2) replacement of the cylindrical tube model for basic pore space geometry with a new unit cell composed of an angular pore cross section (for capillary-dominated phenomena) connected to slit-shaped spaces with internal surface area (for adsorption-dominated processes).

Methodology used:

A new pore space geometry composed of an angular pore cross section (for capillary processes) connected to slit-shaped spaces with internal surface area (for adsorption processes) offering a more realistic representation of natural porous media with explicit consideration of surface area.

Conclusion reached:

At very high capillary pressure (or low wetting phase saturation) the effects of adsorbed films can be significant. Relations between saturation, capillary pressure and interfacial area were derived for bulk-flow, corner-flow and film-flow regimes.

Comments:

It is a means for development of more realistic conceptual models.

---

## Transport in Porous Media, 40, 295-322 (2000)

### Pore Scale Modeling of Rate Effects in Imbibition

Authors: Hughes, R.G.; Blunt, M. J.

Contribution to the understanding of pore network modelling:

Use of a perturbative approach for the rates simulation in a network model. Present a threshold capillary pressure for snap-off for regular polygons.

Two of the five flow regimes (ramified cluster growth and dendritic frontal advance) are described for the first time.

Objectives of the paper:

Study rate effects in imbibition.

Methodology used:

Use of a square or cubic lattice of pores connected by throats

Conclusion reached:

There are five flow patterns observed: (1) bond percolation (as seen by Lenormand and Zarccone, 1984), (2) flat frontal advance (Lenormand and Zarccone, 1984), (3) compact cluster growth (Lenormand and Zarccone, 1984), and two new types of advance caused by the presence of an initial wetting phase saturation – (4) ramified cluster growth, and (5) dendritic frontal advance.

*Ramified cluster growth* occurs at low flow rates and high contact angles, but with significant initial wetting phase saturation. The filled pores and throats that make up the initial saturation of the system are pre-existing sites for the growing clusters. Because of the large number of already-filled elements, each cluster has a ramified or ragged shape, in contrast to the smoother, more compact clusters in compact cluster growth.

*Dendritic frontal advance* occurs when the contact angle is moderate to large, the capillary number is high and an initial wetting phase saturation is present. This regime is similar to frontal advance, in that there is little snap-off and piston-like advance dominates. However, the presence of an initial wetting phase saturation allows a more ramified advance, with significantly more trapping due to bypassing. The width of the wetting front is 10 pore lengths or more.

Comments:

The model accounts for flow in wetting layers that occupy roughness or crevices in the pore space.

---

**Current Opinion in Colloid and Interface Science, 6, 197-207 (2001)****Flow in porous media -- pore-network models and multiphase flow**

Authors: Blunt, M. J.

Contribution to the understanding of pore network modelling:

Summary of what has been done until then in pore-scale modelling.

Objectives of the paper:

Highlight the major advances in pore-scale modelling.

Methodology used:

Literature review

Conclusion reached:

Pore-scale modelling of multiphase flow in porous media is able to explain and interpret experimental results for a wide variety of different situations, including the effects of wettability in two- and three phase flow, multiphase flow in fractures, mass transfer and the influence of flow rate on residual oil saturation.

With realistic descriptions of the pore space, dependent on statistical or explicit reconstruction of a topologically disordered three-dimensional pore space, or through tuning network model parameters to match available data, predictions of properties can be made.

More research is needed to determine if we can characterize the pore space and wettability of reservoir rocks with sufficient ease and accuracy to make predictions of relative permeability and other properties a practical reality. If this is possible, then pore scale modelling will have a huge impact on improved core analysis and characterization of multiphase flow properties.

Comments:

Good review of the research that has been done on pore-scale modelling.

**SPE 71310, 144 (2001)**

## **Verification of a Complete Pore Network Simulator of Drainage and Imbibition**

Authors: Patzek, T. W.

### Contribution to the understanding of pore network modelling:

Example of a 3D quasi static network model, based on realistic representation of actual sandstone morphology, used to predict laboratory measured imbibition relative permeabilities. It comes up with new hydraulic conductance correlations.

### Objectives of the paper:

Summarize the development of a complete quasi static pore-network simulator of two-phase flow, and its validation against a Statoil simulator.

### Methodology used:

The unknown pressures of the interior nodes are calculated from the following system of equations:

$$p_i \left( \sum_{k_i} \frac{g_{i,k_i}}{l_{i,k_i}} \right) - \sum_{k_i} \left( \frac{g_{i,k_i}}{l_{i,k_i}} \right) p_{k_i} = 0 \quad \text{and} \quad p_N \left( \sum_{k_N} \frac{g_{N,k_N}}{l_{N,k_N}} \right) - \sum_{k_N} \left( \frac{g_{N,k_N}}{l_{N,k_N}} \right) p_{k_N} = 0.$$

*l* the spacing between the pore-body centers and *g<sub>i,j</sub>*

the hydraulic conductance

### Conclusion reached:

ANetSim predicts successfully the absolute rock permeability, and the relative permeabilities in primary and higher-order drainage processes. Secondary and higher-order imbibition relative permeabilities are also predicted in good agreement with Statoil's calculations and experiments.

### Comments:

The difference with Oren et al. (1998)'s work is that pore conductances expressions are different.

---

**Advances in Water Resources, 25, 1069 (2002)****Detailed physics, predictive capabilities and macroscopic consequences for pore-network models of multiphase flow**

Authors: Blunt, M. J.; Jackson, M. D.; Piri, M.; Valvatne, P.H.

Contribution to the understanding of pore network modelling:

An example of a quasi-static network model, based on realistic representations of actual sandstone morphology, that ignore rate effects used to predict laboratory measured imbibition relative permeabilities.

Objectives of the paper:

Present a conceptual framework for modelling two- and three-phase flow in geologically realistic networks.

Methodology used:

Pore-network models represented by the pores and throats which are assigned some idealized geometry and rules are developed to determine the multiphase fluid configurations and transport in these elements. The rules are combined in the network to compute effective transport properties on a mesoscopic scale some tens of pores across.

Conclusion reached:

For a water-wet sandstone it was showed that it was possible to predict relative permeability. Physically-derived relative permeabilities can give very different predictions of macroscopic oil recovery from conventional models of relative permeability and hysteresis.

Comments:

The limitation of the quasi-static model used in imbibitions is the treatment of wetting film or corner flow and snap-off.

---

**Journal of Petroleum Science and Engineering, 39, 231 (2002)****Prediction of wettability variation and its impact on flow using pore- to reservoir-scale simulations**

Authors: Jackson, M. D.; Valvatne, P.H.; Blunt, M. J.

Contribution to the understanding of pore network modelling:

Get a wider picture of what pore-scale modelling can help achieve.

Objectives of the paper:

Investigate and predict the effect of wettability variations on flow at the reservoir-scale, using a pore-scale network model in conjunction with reservoir-scale conventional simulations.

Demonstrate that network models of real rocks may be used as a tool to predict wettability variations and their impact on field-scale flow.

Methodology used:

They used a 3-D network model, which combines a physically based pore-scale model of wettability alteration (Blunt, 1998) with a network representation of a Berea sandstone (Bakke and Øren, 1997; Øren et al., 1998; Øren and Bakke, 2002).

They then used a conventional simulator to predict relative permeability and the impact of wettability variations on waterflood efficiency

Conclusion reached:

Proper inclusion of hysteresis is important to predict recovery if wettability varies with height above the OWC.

Using the network model to generate relative permeability curves yields a significantly higher recovery than using empirical models.

Comments:

It was assumed that wettability variations resulted only from variations in the initial water saturation following primary drainage.

---

**Journal of Petroleum Science and Engineering, 39, 177 (2003)****Reconstruction of Berea sandstone and pore-scale modelling of wettability effects**

Authors: Øren, P.-E.; Bakke, S.

Contribution to the understanding of pore network modelling:

Example of reconstruction of a 3D porous media representing Berea sandstone.

Objective of the paper:

Reconstruct 3D Berea sandstone and compare its structure and properties with experiments.

Methodology used:

Utilisation of image analyses of 2D thin section sections to generate a reliable reconstruction of the complex rock-pore system in 3-D (Oren et al.1998).

Conclusion reached:

A quantitative comparison between the experimental microstructure of a Berea sandstone and a reconstructed model shows that porosity distributions and connectivity, are adequately captured in the reconstruction. The topologically equivalent network model accurately predicted both two-phase and three-phase relative permeabilities of water wet Berea.

Comments:

There is no direct evidence that the characterization of wettability on the pore scale is accurate. The method is not applicable to the reconstruction of more heterogeneous and complex rocks that can be found in the oil industry.



---

**SPE 84550, (2003)**

**Predictive Pore-Scale Network Modelling**

Authors: Valvatne, P.H.; Blunt, M. J.

Contribution to the understanding of pore network modelling:

Another example of pore network modelling.

Objectives of the paper:

Show that with easily acquired data difficult to measure properties can be predicted via pore-scale modelling.

Methodology used:

With a network representation of Berea sandstone the pore-size distribution is adjusted to match mercury injection capillary pressure for different rock types, keeping the rank order of pore sizes and the network topology fixed. Then predictions of single and multiphase properties are made with no further adjustment of the model

Conclusion reached:

A realistic network topology combined with network properties tuned to experimental data such as mercury injection capillary pressure is sufficient to predict single and multiphase properties for a wide range of rock types.

Comments:

The limitation of the quasi-static model used in imbibitions is the treatment of wetting film or corner flow and snap-off.

**SPE 90365 (2004)****A Dynamic Network Model for Imbibition**

Authors: Nguyen, V. H.; Sheppard, A. P.; Knackstedt, M. A.; Pinczewski, V. W.

Contribution to the understanding of pore network modelling:

This paper helps to understand the effect of displacement rate on imbibition patterns, relative permeabilities and residual saturations.

Objective of the paper:

Study the effect of displacement rate on imbibition patterns, relative permeabilities and residual saturations

Methodology used:

This paper presents a new network model for imbibition that incorporates a rigorous treatment of the complex dynamics of film flow, swelling and snap-off. The significant difference between this formulation and the quasi-static and dynamic models is the treatment of wetting films. Here, pores and throats have square cross sections.

Conclusion reached:

1. The swelling of wetting films is a capillary pressure driven non-linear diffusion process. The filling of pores and throats ahead of the front as a result of snap-off and snap-off nucleated displacements is therefore a relatively slow process. On the other hand, the time required for piston-like displacements at a connected displacement front depends on displacement rate which may be fast or slow. This is the essence of the rate dependent competition between frontal displacements and snap-off.
2. For very low rates ( $CA < 10^{-8}$ ) the displacement time is very long and there is sufficient time for films to swell significantly throughout the network. Film swelling and snap-off are the dominant displacement mechanisms at low rates and the displacement pattern is similar to bond percolation.
3. For very high rates ( $CA > 10^{-2}$ ) the displacement time is insufficient for films to swell significantly and snap-off may be completely suppressed. The imbibition is dominated by frontal pore and throat filling and the displacement pattern is similar to invasion percolation.
4. For intermediate rates ( $10^{-6} < CA < 10^{-3}$ ) frontal displacements, film swelling, snap-off and snap-off nucleated displacements are all important in determining the displacement pattern.
5. The distance from the front to which the network is affected by film swelling and snap-off decreases with increasing rate.

Comments:

**SPE 95953 (2005)****The Effects of Displacement Rate and Wettability on Imbibition Relative Permeabilities**

Authors: Nguyen, V. H.; Sheppard, A. P.; Knackstedt, M. A.; Pinczewski, V. W.

Contribution to the understanding of pore network modelling:

Another paper on pore network modelling that illustrates how the displacement rate and wettability affect the imbibition relative permeability.

Objective of the paper:

Investigate the effects of displacement rate and wettability on imbibition relative permeability.

Methodology used:

The dynamic network model is the one used in Nguyen et al. (SPE 90365).

Conclusion reached:

1. Displacement rate and contact angle affect the shape of imbibition relative permeability curves in a similar manner. Increasing contact angle and increasing rate increase relative permeability and decrease residual saturation.
2. The sensitivity of relative permeability to displacement rate and contact angle depends on the pore/throat aspect ratio. The sensitivity to rate is high for large aspect ratios and low for small aspect ratios.
3. The complex interaction between displacement rate, contact angle, aspect ratio and pore shape makes it difficult to correctly interpret measured imbibition relative permeability data.

Comments:

---

**Transp Porous Med., 83, 151–169 (2010)**

**Pore-Scale Modelling of Rate Effects in Waterflooding**

Authors: Idowu, N.A.; Blunt, M.J.

Contribution to the understanding of pore network modelling:

A new rule-based, rate-dependent pore-network model has been developed by extending the Hughes and Blunt (2000) perturbative method.

Objectives of the paper:

Study the effects of capillary number  $N_{cap}$ , mobility ratio  $M$  and contact angle distribution on the saturation profiles.

Methodology used:

A dependent network model that accounts for viscous forces by solving for the wetting and non-wetting phase pressure and which allows wetting layer swelling near an advancing flood front.

Conclusion reached:

By using large networks generated using a novel stochastic method, Buckley–Leverett solutions were reproduced, where saturation profiles at different time fall on the same curve when plotted as a function of velocity, directly from pore-scale modelling, thereby providing a bridge between pore-scale and macro-scale transport.

Comments:

It is not capable of simulating ganglion dynamics.

---

**J. Fluid Mech., 655, 38-71 (2010)**

**Non-equilibrium effects in capillarity and interfacial area in two-phase flow: dynamic pore-network modelling**

Authors: Joekar-Niasar, V.; Hassanizadeh, S.M.; Dahle, H.K.

Contribution to the understanding of pore network modelling:

Included the effect of the interfacial area at the oil/water interphase.

Objectives of the paper:

Develop a new dynamic pore-network simulator for two-phase flow in porous media in order to investigate macroscopic relationships among average capillary pressure, average phase pressures, saturation and specific interfacial area.

Methodology used:

They developed a pore-network model with a new computational algorithm, which considers capillary diffusion. Pressure field is calculated for each fluid separately, and saturation is computed in a semi-implicit way. This provides more numerical stability, compared with previous models, especially for unfavourable viscosity ratios and small capillary number values.

Conclusion reached:

At macroscale, average capillary pressure–saturation–interfacial area points fall on a single surface regardless of flow conditions and fluid properties.

They show that the traditional capillary pressure–saturation relationship is not valid under dynamic conditions, as predicted by the theory. The non-equilibrium capillary theory needs to be employed, according to which the fluids pressure difference is a function of the time rate of saturation change

Comments:

The model is only applied to a small domain.

---

**16th European Symposium on Improved Oil Recovery, Cambridge, UK, 12-14 Apr. (2011)****Effects of Surfactant on Wettability and Oil Recovery in a Pore Network Model**

Authors: Unsal, E.; Hammond, P.S.; Schneider, M.

Contribution to the understanding of pore network modelling:

Modelled the injection of surfactant solution.

Objectives of the paper:

Present a dynamic model, capable of predicting the displacement of oil by surfactant solution within a network representation of the void space of a porous solid medium.

Methodology used:

A dynamic network model for the displacement of oil by aqueous phase taking account of capillary and viscous effects, a simulation of the transport of surfactant through the network by advection and diffusion taking account of adsorption on the solid surface, and the coupling of these two by linking the contact angle and interfacial tension appearing in the dynamic network simulation to the local concentration of surfactant computed in the transport simulation.

Conclusion reached:

The model reproduces the displacement patterns observed by other authors in two-dimensional networks as capillary number and mobility ratio are varied.

Surfactant alters the wettability and the interfacial tension and may have a stabilizing effect when the viscous forces are not very significant. It changes the displacement pattern in favor of oil recovery.

Comments:

It is not capable of simulating ganglion dynamics

---

**Transp Porous Med., 92, 789–817 (2012)**

**A Dynamic Pore Network Model for Oil Displacement by Wettability-Altering Surfactant Solution**

Authors: Hammond, P.S.; Unsal, E.

Contribution to the understanding of pore network modelling:

Modelled the injection of surfactant solution and wettability alteration.

Objectives of the paper:

Present a dynamic model, capable of predicting the displacement of oil by surfactant solution within a network representation of the void space of a porous solid medium.

Methodology used:

A dynamic network model for the displacement of oil by aqueous phase taking account of capillary and viscous effects, a simulation of the transport of surfactant through the network by advection and diffusion taking account of adsorption on the solid surface, and the coupling of these two by linking the contact angle and interfacial tension appearing in the dynamic network simulation to the local concentration of surfactant computed in the transport simulation.

Conclusion reached:

The model reproduces the displacement patterns observed by other authors in two-dimensional networks as capillary number and mobility ratio are varied.

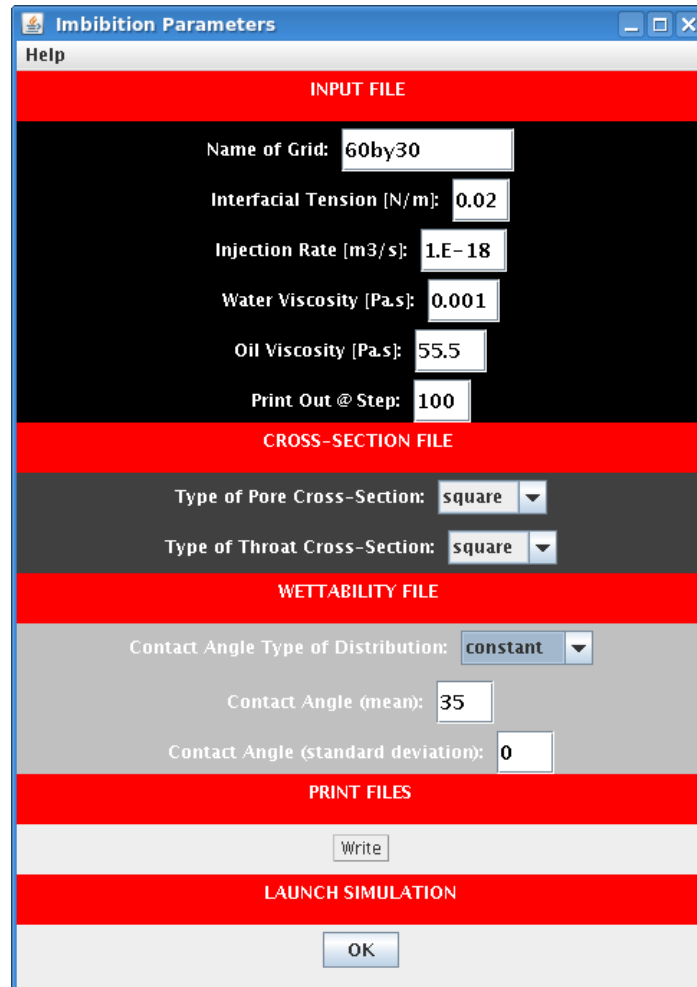
A mechanism is demonstrated whereby in an initially mixed-wet medium, surfactant-induced wettability alteration can lead to stabilization of displacement fronts.

Comments:

It is not capable of simulating ganglion dynamics

## Appendix B – User Interface

To make the code more user friendly, the simulations were allowed to be run through interactive windows (Figure B- 1). Before that improvement, all the parameters, that are the oil and water viscosities, the contact angle, the shapes of the cross-sections of the pores and throats, the injection rate at which the water is injected or the interfacial tension, had to be entered manually inside the code itself. It is now easier to launch simulations and all of the parameters entered can be understood by going through the help guidance window (Figure B- 2).



The screenshot shows a window titled "Imbibition Parameters" with a "Help" button in the top-left corner. The window is divided into several sections by red horizontal bars:

- INPUT FILE** (red bar):
  - Name of Grid:
  - Interfacial Tension [N/m]:
  - Injection Rate [m<sup>3</sup>/s]:
  - Water Viscosity [Pa.s]:
  - Oil Viscosity [Pa.s]:
  - Print Out @ Step:
- CROSS-SECTION FILE** (red bar):
  - Type of Pore Cross-Section:  (dropdown menu)
  - Type of Throat Cross-Section:  (dropdown menu)
- WETTABILITY FILE** (red bar):
  - Contact Angle Type of Distribution:  (dropdown menu)
  - Contact Angle (mean):
  - Contact Angle (standard deviation):
- PRINT FILES** (red bar):
  -
- LAUNCH SIMULATION** (red bar):
  -

Figure B- 1: Window in which you enter the imbibition parameters you wish to run your simulation for.



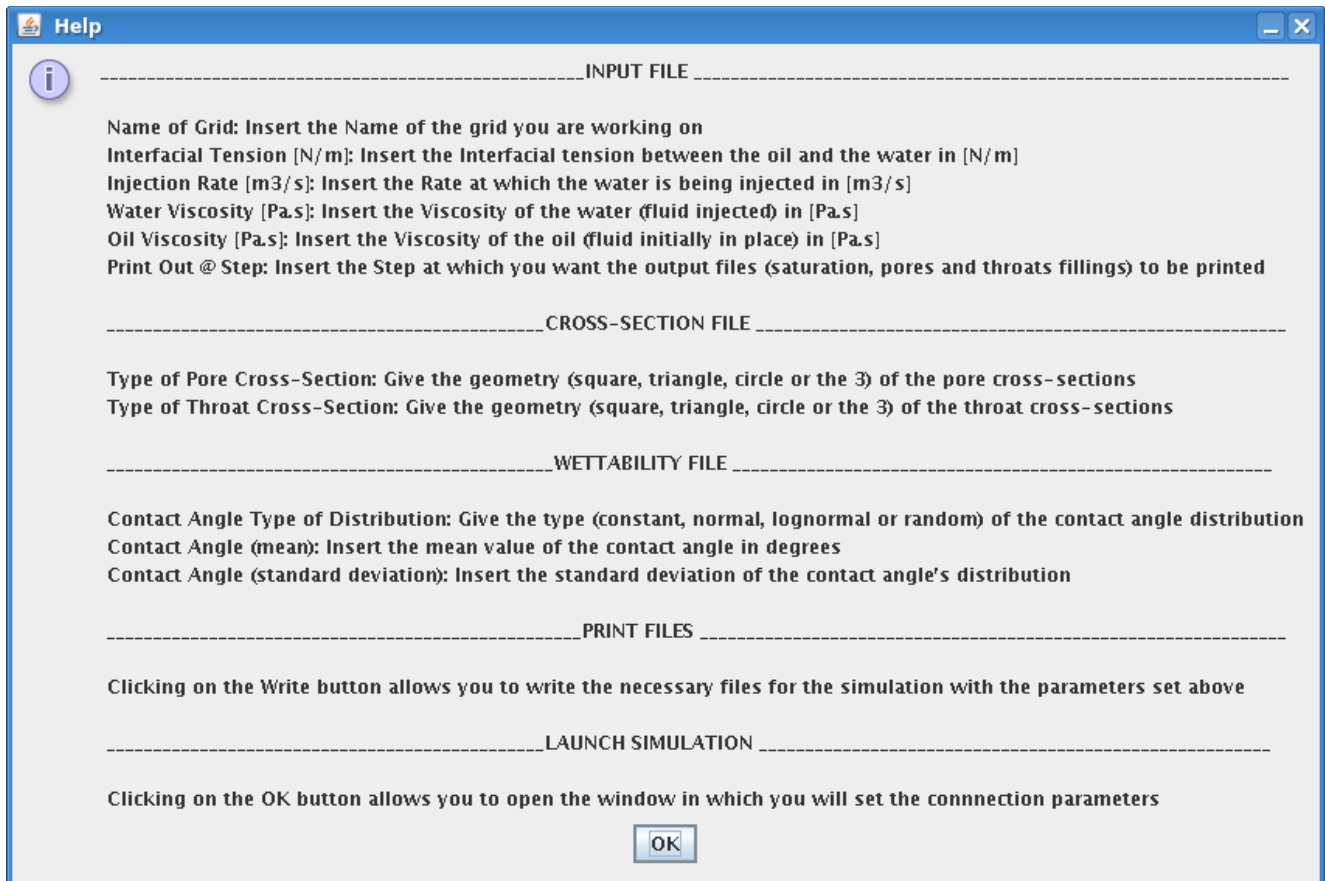


Figure B- 2: Help window explaining what all the imbibition parameters correspond to.

It is also now possible to select the type of contact angle distribution desired: it can be set constant for the entire network, follow a normal or lognormal type of distribution or they can be randomly assigned throughout the network.

### Appendix C – 100\*100 network simulation

The first series of simulation for the 100\*100 grid was done at a constant  $\log M = -4.7$ . The parameters that were used are listed in Table C- 1.

Table C- 1: Parameters used for the 100\*100 simulations at a constant  $\log M = -4.7$

Name	$\mu_w$ (Pa.s)	$\mu_o$ (Pa.s)	ift (N/m)	$q_w$ (m <sup>3</sup> /s)	A (m <sup>2</sup> )	cos ( $\theta$ )	M	log M	Ca	log Ca	$S_{win}$
100by100_a1	1.8E-05	1	2E-02	2.0E-07	9.98E-05	0.82	1.8E-05	-4.7	2.2E-06	-5.7	0.014
100by100_a2	1.8E-05	1	2E-02	2.0E-08	9.98E-05	0.82	1.8E-05	-4.7	2.2E-07	-6.7	0.014
100by100_a3	1.8E-05	1	2E-02	8.0E-10	9.98E-05	0.82	1.8E-05	-4.7	8.8E-09	-8.1	0.023
100by100_a4	1.8E-05	1	2E-02	2.0E-10	9.98E-05	0.82	1.8E-05	-4.7	2.2E-09	-8.7	0.038
100by100_a5	1.8E-05	1	2E-02	2.0E-11	9.98E-05	0.82	1.8E-05	-4.7	2.2E-10	-9.7	0.136
100by100_a6	1.8E-05	1	2E-02	2.0E-12	9.98E-05	0.82	1.8E-05	-4.7	2.2E-11	-10.7	0.261
100by100_a7	1.8E-05	1	2E-02	2.0E-13	9.98E-05	0.82	1.8E-05	-4.7	2.2E-12	-11.7	0.309
100by100_a8	1.8E-05	1	2E-02	2.0E-14	9.98E-05	0.82	1.8E-05	-4.7	2.2E-13	-12.7	0.316

To be able to see a capillary fingering plateau in the injected fluid saturation profile, simulations on lower capillary numbers than  $\log Ca = -10.7$  had to be done. The flow patterns corresponding to capillary fingering that were achieved can be seen in Figure C- 1. The green represents the non-wetting fluid in place and in blue the wetting fluid injected.

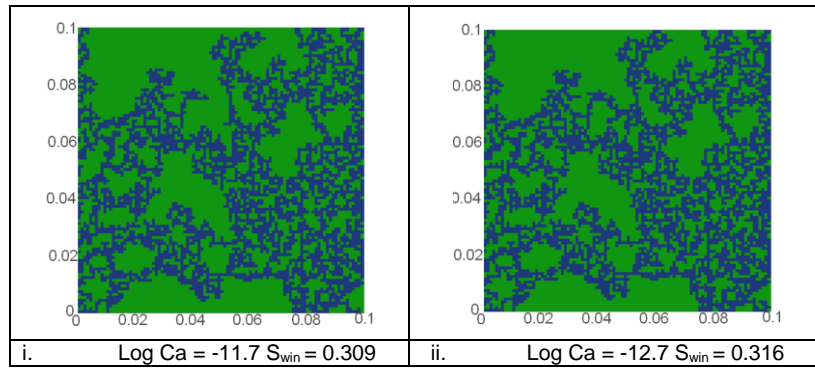


Figure C- 1: 100\*100 simulations while varying the capillary numbers: (a)  $\log M = -4.7$ . Small Ca are simulated in order to reach the capillary fingering plateau.

The second series of simulation for the 100\*100 grid was done at a constant  $\log M = 1.9$ . The parameters that were used are listed in.

The third series of simulation for the 100\*100 grid was done at a constant  $\log Ca = 0$ . The parameters that were used are listed in Table C- 2.

Table C- 2: Parameters used for the 100\*100 simulations at a constant  $\log Ca = 0$

Name	$\mu_w$ (Pa.s)	$\mu_o$ (Pa.s)	ift (N/m)	$q_w$ (m <sup>3</sup> /s)	A (m <sup>2</sup> )	cos ( $\theta$ )	M	log M	Ca	log Ca	$S_{win}$
100by100_c1	1E+00	1E+04	2E-02	1.64E-06	9.98E-05	0.82	0.0001	-4	1.0E+00	0	0.014
100by100_c2	1E+00	1E+02	2E-02	1.64E-06	9.98E-05	0.82	0.01	-2	1.0E+00	0	0.014
100by100_c3	1E+00	1E+01	2E-02	1.64E-06	9.98E-05	0.82	0.1	-1	1.0E+00	0	0.103
100by100_c4	1E+00	1E+00	2E-02	1.64E-06	9.98E-05	0.82	1	0	1.0E+00	0	0.610
100by100_c5	1E+00	1E-02	2E-02	1.64E-06	9.98E-05	0.82	100	2	1.0E+00	0	0.920
100by100_c6	1E+00	1E-04	2E-02	1.64E-06	9.98E-05	0.82	10000	4	1.0E+00	0	0.920

To be able to see a piston-like displacement plateau in the injected fluid saturation profile, a simulation with a viscosity ratio of 10,000 was done. The piston-like displacement gotten can be seen in Figure C- 2.

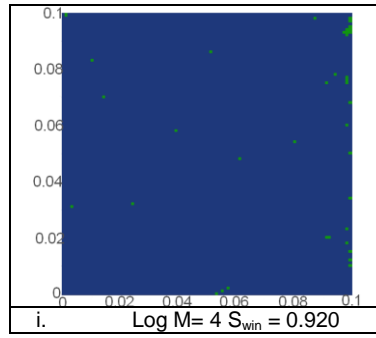


**Figure C- 2: 100\*100 simulation while varying the viscosity ratios: (c)  $\log Ca = 0$ .  
A big viscosity ratio is simulated in order to reach the piston-like displacement plateau**

## Appendix D – 25\*25 network simulation

To obtain the saturation profile presented, four series of simulations were run.

The first series of simulation for the 25\*25 grid was done at a constant  $\log M = -4.7$ . The parameters that were used are listed in Table D- 1.

Table D- 1: Parameters used for the 25\*25 simulations at a constant  $\log M = -4.7$

Name	$\mu_w$ (Pa.s)	$\mu_o$ (Pa.s)	ift (N/m)	$q_w$ (m <sup>3</sup> /s)	A (m <sup>2</sup> )	cos ( $\theta$ )	M	log M	Ca	log Ca	$S_{win}$
25by25_a1	1.8E-05	1	2E-02	5.2E-08	2.58E-05	0.82	1.8E-05	-4.7	2.2E-06	-5.7	0.07
25by25_a2	1.8E-05	1	2E-02	5.2E-09	2.58E-05	0.82	1.8E-05	-4.7	2.2E-07	-6.7	0.07
25by25_a3	1.8E-05	1	2E-02	2.1E-10	2.58E-05	0.82	1.8E-05	-4.7	8.9E-09	-8.0	0.08
25by25_a4	1.8E-05	1	2E-02	5.2E-11	2.58E-05	0.82	1.8E-05	-4.7	2.2E-09	-8.7	0.12
25by25_a4bis	1.8E-05	1	2E-02	1.4E-11	2.58E-05	0.82	1.8E-05	-4.7	6.0E-10	-9.2	0.21
25by25_a5	1.8E-05	1	2E-02	5.2E-12	2.58E-05	0.82	1.8E-05	-4.7	2.2E-10	-9.7	0.44
25by25_a6	1.8E-05	1	2E-02	5.2E-13	2.58E-05	0.82	1.8E-05	-4.7	2.2E-11	-10.7	0.44
25by25_a7	1.8E-05	1	2E-02	5.2E-14	2.58E-05	0.82	1.8E-05	-4.7	2.2E-12	-11.7	0.43

To see an entire saturation profile between the viscous fingering and the capillary fingering plateaus the flow patterns seen in Figure D- 1 came out.

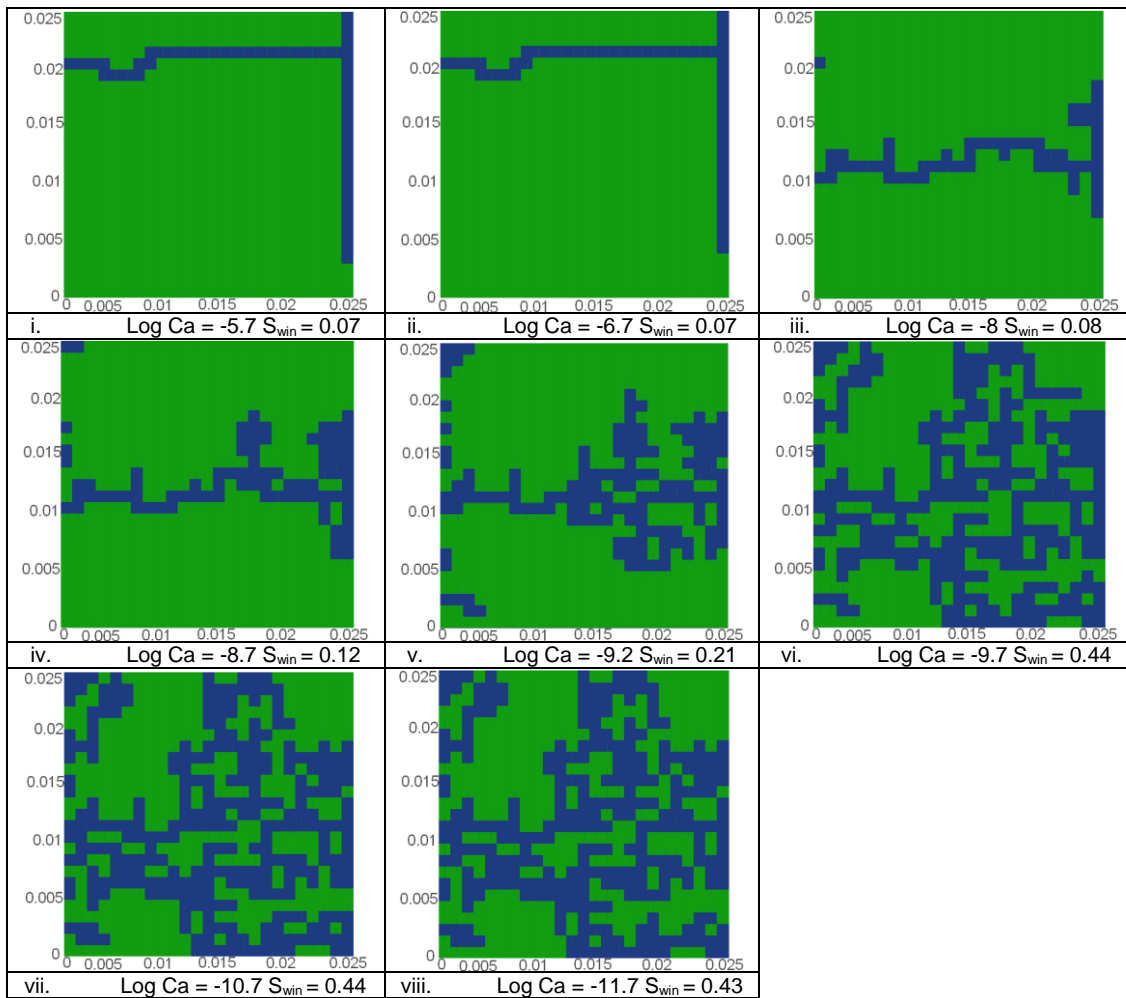


Figure D- 1: 25\*25 simulations while varying the capillary numbers: (a)  $\log M = -4.7$ . Small Ca are simulated in order to reach the capillary fingering plateau.

The second series of simulation for the 25\*25 grid was done at a constant  $\log M = 1.9$ . The parameters that were used are listed in Table D- 2.

Table D- 2: Parameters used for the 25\*25 simulations at a constant log M = 1.9

Name	$\mu_w$ (Pa.s)	$\mu_o$ (Pa.s)	ift (N/m)	$q_w$ (m <sup>3</sup> /s)	A (m <sup>2</sup> )	cos ( $\theta$ )	M	log M	Ca	log Ca	$S_{win}$
25by25_b0	1.6E-03	1.8E-05	2E-02	2.7E-04	2.58E-05	0.8192	86	1.9	1.00E+00	0.0	0.68
25by25_b1bis	1.6E-03	1.8E-05	2E-02	8.0E-05	2.58E-05	0.8192	86	1.9	2.93E-01	-0.5	0.68
25by25_b1	1.6E-03	1.8E-05	2E-02	3.1E-05	2.58E-05	0.8192	86	1.9	1.14E-01	-0.9	0.68
25by25_b2	1.6E-03	1.8E-05	2E-02	3.1E-06	2.58E-05	0.8192	86	1.9	1.14E-02	-1.9	0.51
25by25_b3	1.6E-03	1.8E-05	2E-02	3.1E-08	2.58E-05	0.8192	86	1.9	1.14E-04	-3.9	0.5
25by25_b4	1.6E-03	1.8E-05	2E-02	3.1E-09	2.58E-05	0.8192	86	1.9	1.14E-05	-4.9	0.41
25by25_b5	1.6E-03	1.8E-05	2E-02	3.1E-10	2.58E-05	0.8192	86	1.9	1.14E-06	-5.9	0.54
25by25_b6	1.6E-03	1.8E-05	2E-02	3.1E-11	2.58E-05	0.8192	86	1.9	1.14E-07	-6.9	0.48
25by25_b7	1.6E-03	1.8E-05	2E-02	3.1E-12	2.58E-05	0.8192	86	1.9	1.14E-08	-7.9	0.49
25by25_b8	1.6E-03	1.8E-05	2E-02	3.1E-13	2.58E-05	0.8192	86	1.9	1.14E-09	-8.9	0.49

To see an entire saturation profile between the piston-like displacement and viscous fingering plateaus the flow patterns seen in Figure D- 2 came out. The grid issue is present in this run of simulations as the piston-like displacement stops abruptly in the middle of its path towards the exit.

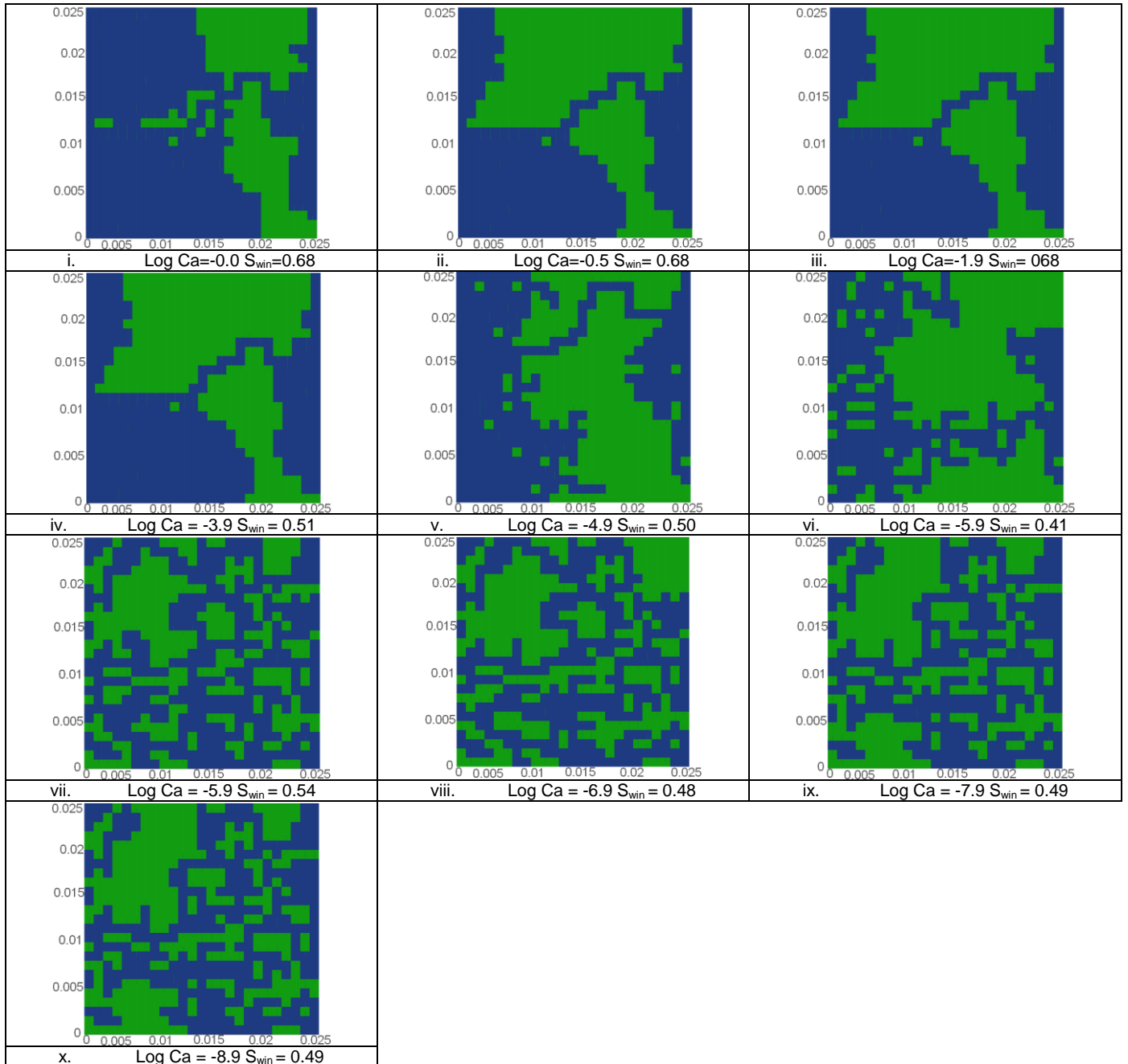


Figure D- 2: 25\*25 simulations while varying the capillary numbers: (a) log M = 1.9. Small Ca are simulated in order to reach the capillary fingering plateau.

The third series of simulation for the 25\*25 grid was done at a constant  $\log Ca = 0$ . The parameters that were used are listed in Table D- 3.

Table D- 3: Parameters used for the 25\*25 simulations at a constant  $\log Ca = 0$

Name	$\mu_w$ (Pa.s)	$\mu_o$ (Pa.s)	ift (N/m)	$q_w$ (m <sup>3</sup> /s)	A (m <sup>2</sup> )	cos ( $\theta$ )	M	log M	Ca	log Ca	$S_{win}$
25by25_c1	1	1E+04	2E-02	4.2E-07	2.58E-05	0.82	0.0001	-4	1	0	0.07
25by25_c2	1	1E+02	2E-02	4.2E-07	2.58E-05	0.82	0.01	-2	1	0	0.07
25by25_c3	1	1E+01	2E-02	4.2E-07	2.58E-05	0.82	0.1	-1	1	0	0.13
25by25_c4bis	1	3E+00	2E-02	4.2E-07	2.58E-05	0.82	0.31623	-0.5	1	0	0.17
25by25_c4	1	1E+00	2E-02	4.2E-07	2.58E-05	0.82	1	0	1	0	0.62
25by25_c5bis	1	1E-01	2E-02	4.2E-07	2.58E-05	0.82	10	1	1	0	0.67
25by25_c5	1	1E-02	2E-02	4.2E-07	2.58E-05	0.82	100	2	1	0	0.68
25by25_c6bis	1	1E-03	2E-02	4.2E-07	2.58E-05	0.82	1000	3	1	0	0.68
25by25_c6	1	1E-04	2E-02	4.2E-07	2.58E-05	0.82	10000	4	1	0	0.68

To be able to see from the viscous fingering to the piston-like displacement plateaus in the injected fluid saturation profile, the simulations that can be seen in Figure D- 3 were run.

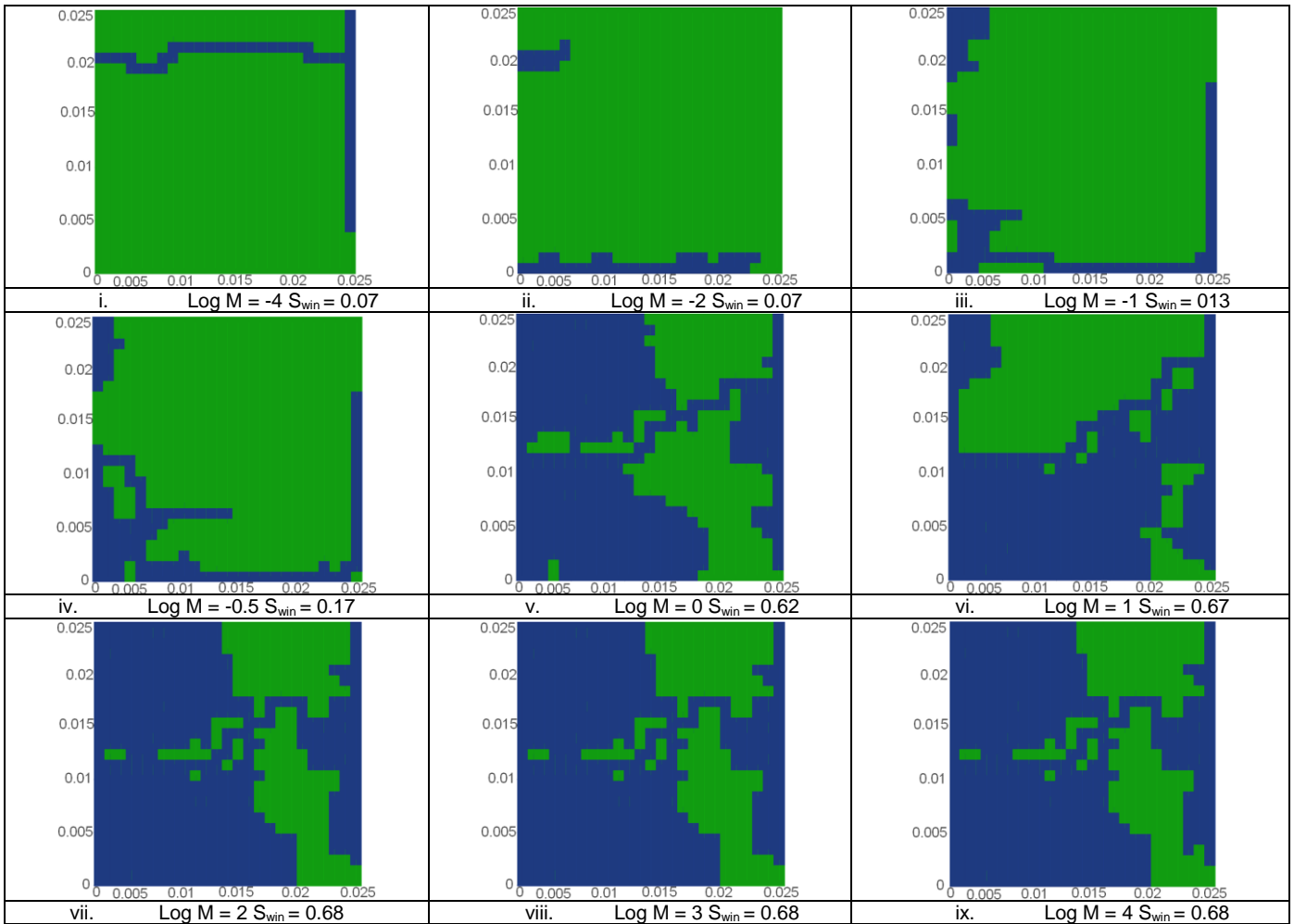


Figure D- 3: 25\*25 simulation while varying the viscosity ratios: (c)  $\log Ca = 0$ . A big viscosity ratio is simulated in order to reach the piston-like displacement plateau

The fourth series of simulation for the 25\*25 grid was done at a constant  $\log Ca = -6.5$ . The parameters that were used are listed in Table D- 4.

Table D- 4: Parameters used for the 25\*25 simulations at a constant log Ca = -6.5

Name	$\mu_w$ (Pa.s)	$\mu_o$ (Pa.s)	ift (N/m)	$q_w$ (m <sup>3</sup> /s)	A (m <sup>2</sup> )	cos ( $\theta$ )	M	log M	Ca	log Ca	$S_{win}$
25by25_d-1	1	1E+06	2E-02	1.3E-13	2.58E-05	0.8192	1E-06	-6	3E-07	-6.5	0.07
25by25_d0	1	1E+05	2E-02	1.3E-13	2.58E-05	0.8192	0.00001	-5	3E-07	-6.5	0.07
25by25_d1	1	1E+04	2E-02	1.3E-13	2.58E-05	0.8192	0.0001	-4	3E-07	-6.5	0.06
25by25_d1bis	1	1E+03	2E-02	1.3E-13	2.58E-05	0.8192	0.001	-3	3E-07	-6.5	0.11
25by25_d2	1	1E+02	2E-02	1.3E-13	2.58E-05	0.8192	0.01	-2	3E-07	-6.5	0.34
25by25_d3	1	1E+01	2E-02	1.3E-13	2.58E-05	0.8192	0.1	-1	3E-07	-6.5	0.48
25by25_d4	1	3E+00	2E-02	1.3E-13	2.58E-05	0.8192	0.31623	-0.5	3E-07	-6.5	0.51
25by25_d5	1	1E+00	2E-02	1.3E-13	2.58E-05	0.8192	1	0	3E-07	-6.5	0.51
25by25_d7	1	1E-02	2E-02	1.3E-13	2.58E-05	0.8192	100	2	3E-07	-6.5	0.51

To be able to see from the viscous fingering to the capillary fingering plateaus in the injected fluid saturation profile, the simulations that can be seen in Figure D- 4 were run.

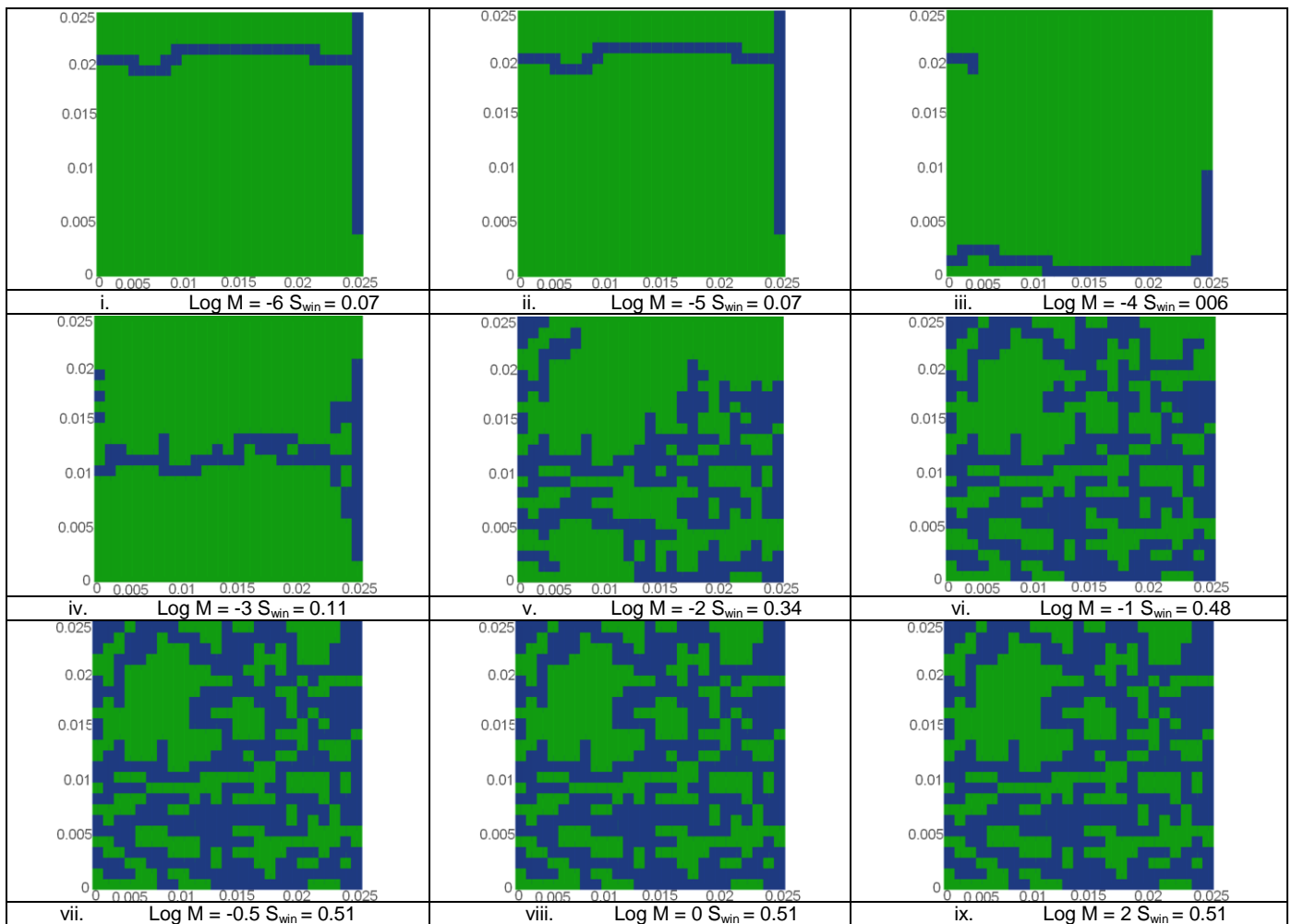


Figure D- 4: 25\*25 simulation while varying the viscosity ratios: (c) log Ca = -6.5. A small viscosity ratio is simulated in order to reach the viscous fingering plateau

## Appendix E – 3D Simulations

The parameters used for the 3D network model simulations are listed in the Table E- 1 and Table E- 2.

Table E- 1: Parameters used for the 3D simulations at a constant log M = -2

Name	$\mu_w$ (Pa.s)	$\mu_o$ (Pa.s)	ift (N/m)	$q_w$ (m <sup>3</sup> /s)	A (m <sup>2</sup> )	cos ( $\theta$ )	M	log M	Ca	log Ca	$S_{win}$
C1_a-1	1.00E-02	1.00E+00	2.00E-02	1.00E-07	5.70E-06	0.819152	0.01	-2.0	1.07E-02	-2.0	0.338
C1_a0	1.00E-02	1.00E+00	2.00E-02	1.00E-08	5.70E-06	0.819152	0.01	-2.0	1.07E-03	-3.0	0.345
C1_a1	1.00E-02	1.00E+00	2.00E-02	1.00E-09	5.70E-06	0.819152	0.01	-2.0	1.07E-04	-4.0	0.34
C1_a2	1.00E-02	1.00E+00	2.00E-02	1.00E-10	5.70E-06	0.819152	0.01	-2.0	1.07E-05	-5.0	0.328
C1_a3	1.00E-02	1.00E+00	2.00E-02	1.00E-11	5.70E-06	0.819152	0.01	-2.0	1.07E-06	-6.0	0.348
C1_a4	1.00E-02	1.00E+00	2.00E-02	1.00E-12	5.70E-06	0.819152	0.01	-2.0	1.07E-07	-7.0	0.504
C1_a5	1.00E-02	1.00E+00	2.00E-02	1.00E-13	5.70E-06	0.819152	0.01	-2.0	1.07E-08	-8.0	0.58
C1_a6	1.00E-02	1.00E+00	2.00E-02	1.00E-14	5.70E-06	0.819152	0.01	-2.0	1.07E-09	-9.0	0.605
C1_a7	1.00E-02	1.00E+00	2.00E-02	1.00E-15	5.70E-06	0.819152	0.01	-2.0	1.07E-10	-10.0	0.622
C1_a8	1.00E-02	1.00E+00	2.00E-02	1.00E-16	5.70E-06	0.819152	0.01	-2.0	1.07E-11	-11.0	0.635
C1_a9	1.00E-02	1.00E+00	2.00E-02	1.00E-17	5.70E-06	0.819152	0.01	-2.0	1.07E-12	-12.0	0.635
C1_a10	1.00E-02	1.00E+00	2.00E-02	1.00E-18	5.70E-06	0.819152	0.01	-2.0	1.07E-13	-13.0	0.635

Table E- 2: Parameters used for the 3D simulations at a constant log M = 2

Name	$\mu_w$ (Pa.s)	$\mu_o$ (Pa.s)	ift (N/m)	$q_w$ (m <sup>3</sup> /s)	A (m <sup>2</sup> )	cos ( $\theta$ )	M	log M	Ca	log Ca	$S_{win}$
C1_b-3	1.00E+00	1.00E-02	2.00E-02	1.00E-07	5.70E-06	0.819152	100	2.0	1.07E+00	0.0	0.721
C1_b-2	1.00E+00	1.00E-02	2.00E-02	1.00E-08	5.70E-06	0.819152	100	2.0	1.07E-01	-1.0	0.721
C1_b-1	1.00E+00	1.00E-02	2.00E-02	1.00E-09	5.70E-06	0.819152	100	2.0	1.07E-02	-2.0	0.728
C1_b0	1.00E+00	1.00E-02	2.00E-02	1.00E-10	5.70E-06	0.819152	100	2.0	1.07E-03	-3.0	0.685
C1_b1	1.00E+00	1.00E-02	2.00E-02	1.00E-11	5.70E-06	0.819152	100	2.0	1.07E-04	-4.0	0.744
C1_b2	1.00E+00	1.00E-02	2.00E-02	1.00E-12	5.70E-06	0.819152	100	2.0	1.07E-05	-5.0	0.806
C1_b3	1.00E+00	1.00E-02	2.00E-02	1.00E-13	5.70E-06	0.819152	100	2.0	1.07E-06	-6.0	0.577
C1_b4	1.00E+00	1.00E-02	2.00E-02	1.00E-14	5.70E-06	0.819152	100	2.0	1.07E-07	-7.0	0.689
C1_b5	1.00E+00	1.00E-02	2.00E-02	1.00E-15	5.70E-06	0.819152	100	2.0	1.07E-08	-8.0	0.647
C1_b6	1.00E+00	1.00E-02	2.00E-02	1.00E-16	5.70E-06	0.819152	100	2.0	1.07E-09	-9.0	0.635
C1_b7	1.00E+00	1.00E-02	2.00E-02	1.00E-17	5.70E-06	0.819152	100	2.0	1.07E-10	-10.0	0.635
C1_b8	1.00E+00	1.00E-02	2.00E-02	1.00E-18	5.70E-06	0.819152	100	2.0	1.07E-11	-11.0	0.635
C1_b9	1.00E+00	1.00E-02	2.00E-02	1.00E-19	5.70E-06	0.819152	100	2.0	1.07E-12	-12.0	0.635
C1_b10	1.00E+00	1.00E-02	2.00E-02	1.00E-20	5.70E-06	0.819152	100	2.0	1.07E-13	-13.0	0.635